Characterization studies of detectors for the search of rare events

A thesis Submitted
in Partial Fulfilment of the Requirements
for the Degree of

MASTER OF SCIENCE

by

SHARADA PRASAD SAHOO

to the

School of physical Sciences

National Institute of Science Education and Research

Bhubaneswar

Date

DECLARATION

I hereby declare that I am the sole author of this thesis in partial fulfillment of the requirements for a postgraduate degree from National Institute of Science Education and Research (NISER). I authorize NISER to lend this thesis to other institutions or individuals for the purpose of scholarly research.

Sharada Prasad Sahoo

Signature of the Student

Date: 12-07-2021

The thesis work reported in the thesis entitled **Characterization studies of detectors for the search of rare events** was carried out under my supervision, in the **school of physical sciences at NISER, Bhubaneswar, India**.

Signature of the thesis supervisor

School:

Date:

ACKNOWLEDGEMENTS

It is a pleasure to express thanks and gratitude to Professor Bedangadas Mohanty who help me guide throughout this research. He has direct and indirect contributions in pushing me to aim towards larger things. Several discussions with him help me to learn some of his perspective towards research work which will surely guide me in my future research. I am extremely thankful to his PhD student Vijay Iyer, he is a mentor to me who guides me throughout the thesis not only in study perspective but also his experience help me in handling the given work. He has been a constant motivation to me in the sense how to maintain calm and cool in different situations. I would also like to thank Dr. Varchaswi Kashyap in helping me to resolve issues from his experience and knowledge. I would like to thank to Bedanga sir's PhD student Mouli Chaudhury for helping me in analysis from her research experience.

ABSTRACT

This thesis work involves characterization of two types of silicon detectors and a sapphire detector, that are used in rare event searches. Thesis begins with the motivation to search for rare events like dark matter, $CE\nu NS$ (coherent elastic neutrino nucleus scattering). It also discuss about the MINER (Mitchell institute neutrino experiment at reactor, Texas) which aims to detect $CE\nu NS$ and sterile neutrino oscillation that could be a possible solution to the dark matter problem. Three detectors which have been described in this thesis are different from each their in some useful properties. Silicon high voltage detector can detect very low energy transfer interactions. Hybrid detector has an important feature that it will be able to discriminate backgrounds which comes due to electrons, photons or neutrons, in addition to low energy detection. Whereas sapphire detector is being used due to it's higher capacity of energy resolution. Data from all these detectors are analyzed and properties of the detectors are discussed with the results.

Contents

List of Figures

List of Tables

Chapter 1

Introduction

Dark matter (DM) and neutrinos are among the most mysterious entities in the Universe. The identity of DM, if it is of particle nature, is yet to be discovered. Several intrinsic properties of neutrinos are still being studied by various experiments around the world [1]. Most direct detection experiments for these particles are built on the principle of measuring recoil energies from an elastic scattering of the particle of a target medium[2]. These particles are elusive to direct detection experiments due to their low interaction cross section with the target material. Additionally, the recoil energy imparted by the scattered particle in the detector is very low i.e. less than 10 keV which makes their measurement challenging [3]. The radioactive and cosmogenic backgrounds from various sources like the U and Th decay chains, and cosmic rays add to the difficulty of identifying recoil energy signals from DM or neutrinos. The combination of low interaction cross section of these particles with the detector material, low recoil energy signals, and presence of other backgrounds make detecting these events rare.

With advances in understanding of backgrounds and high sensitivity sensor materials, science is progressing towards finding new technology to detect the rare events. Different semiconductor detectors like silicon or germanium with superconductor based sensors are used to detect low recoil energy. After understanding the backgrounds, different shielding procedures like lead to block neutrons, polyethylene to block γ rays have been done and also different analysis methods have been proposed to reject backgrounds from the data analysis.

Following sections in this chapter include CEνNS process and details about an experiment built for the detection of CEνNS called Mitchell institute neutrino experiment at reactor (MINER).

1.1 $CE\nu NS$

When an elementary particle (e.g.neutrino) scatters off a composite object (e.g.nucleus), scattering cross section from each of the individual element of the composite particle (nucleon) adds up to give an enhanced scattering cross section. So, probability of occurrence of the event will increase due to coherent addition. This process is similar to all interference phenomenon where waves interfere constructively to give an increase in amplitude of the resultant wave.

If a neutrino having momenta $\vec{k}$ scatter from a rest nucleus with momenta $\vec{k'}$, then scattering amplitude $F(\vec{k}, \vec{k'})$ of the interaction will be[4].

$$F(k, k') = \sum_{A=1}^{N} f_j(k, k') e^{-i(k-k')x_j} \tag{1.1}$$

where $f_j(k, k')$ and x_j are the scattering amplitude and position of the j^{th} nucleon in the nucleus. $CE\nu NS$ holds if the condition $(k - k') \cdot R << 1$ holds, where R is the radius of the nucleus. That means $e^{-i(k-k')\cdot x_j} = \cos((k-k')\cdot x_j) - i\sin((k-k')\cdot x_j) \sim 1$ (as $x_j < R$, the above condition still holds). The total scattering amplitude now is the simple addition of scattering amplitude from all the nucleons. Increased amplitude increases it's probability to interact with SM particles hence the chance of detection, but still scattering cross-section is less comparable to other SM interactions, so careful procedures with advance electronics require to detect the event.

1.1.1 CEνNS as a probe for beyond standard model (BSM) physics

Through the detection of CEνNS, many BSM physics like sterile neutrino oscillation, anomalous neutrino magnetic moment, non-standard interaction etc. can be studied or described.

Some of the experiments like LSND and MiniBooNE have detected excess of the ν_e signal from expected[5], this result might produce due to oscillation of fourth neutrino also called sterile neutrino. Detecting CEνNS might give us some lead to prove the appearance of new neutrino in the theory.

CEνNS is an nuclear recoil process. However there are many electron recoil events produce backgrounds in the process. XENON1T, an experiment which search for dark matter also tried to study the electron recoil events and found an excess of 53 ± 15 events above the expected background. They report that such an excess event is consistent with solar axion-electron coupling and neutrino-electron interaction with large neutrino magnetic moment[6]. Such a theory can be tested with CEνNS based experiments also.

New neutrino interactions or non-standard interaction beyond standard model are prominent features of different neutrino mass models[7]. Presence of non standard interaction might affect their production, propagation in the medium as well as detection by the detector material, hence, can produce unpredictable events beyond standard model in the CEνNS experiment.

1.1.2 CEνNS in dark matter search experiments

CEνNS forms an irreducible background in dark matter search experiment. Detecting and understanding CEνNS will be helpful towards detection of dark matter by removing CEνNS from the background. This section describes the reason for which

we considered CEνNS as an irreducible background. For this we need to learn dark matter detection plot first. It is plotted to search dark matters in different mass versus interaction cross section range and is obtained from the results of different dark matter search experiments.

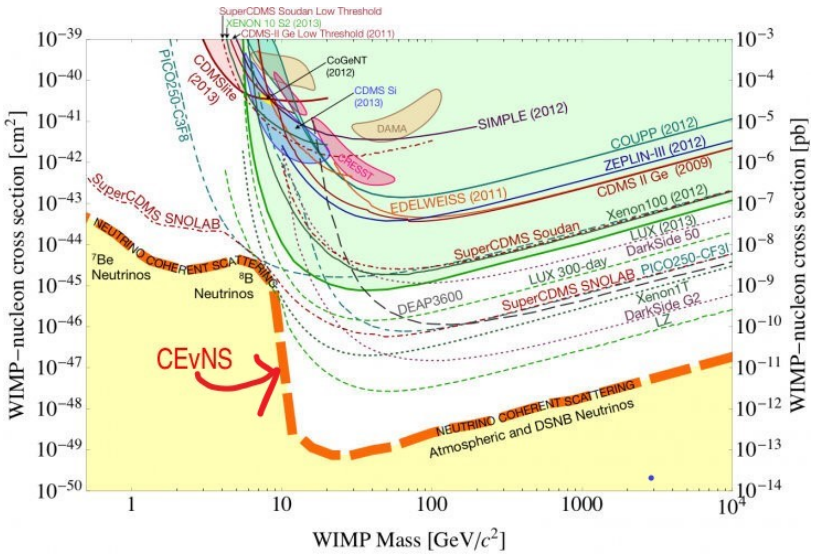

Figure 1.1: Above figure is the scattering cross section versus mass graph for a dark matter candidate called WIMP (Weakly interacting massive particle). Green regions in the top right side of plot suggest no chance of detection of WIMP in the respective mass and cross-section. Small contours in those regions denotes claim of some experiment for the dark matter detection but have not been confirmed yet. White regions suggest unexplored area. Dotted boundaries suggest future explore to that area. Lower part tells that you can not distinguish between neutrino and WIMP interaction, the region is called neutrino floor. Figure courtesy [8]

For heavy mass dark matter with mass ($m >= 10GeV$), detection have been carried out with the help of liquid xenon or liquid argon based detectors.There is no clear evidence for dark matter is found in the high mass range. Green contour in Fig.1.1 suggests that there is no possible signal for dark matter found yet.

Semiconductors like silicon and germanium are used as detectors at very low temperature to detect low mass WIMPs ($m <= 10GeV$). Four contours in the plot suggests that four different experiments e.g. CRESST ($CaWO_4$ target), CDMS (Si target), COGENT (Ge target) and DAMA (NaI target) claim the detection of events

excess than backgrounds, but the possibility of these extra events as dark matter has not been confirmed yet.

The solid lines in the plot represent explored mass and cross section regions for the detection of the dark matter. The dashed line shows the future predictions of different experiments in the range. But while moving forward or towards low mass and cross-section region, CEνNS will start to form an important background. This background also can not be shielded due to their very low scattering cross-section. So they will form an irreducible background in the search of low mass and cross-section dark matters. Their detection may help us to understand more about them and also help us to remove them from the background in the dark matter search experiment.

1.2 MINER

MINER is a reactor based experiment will use improved semiconductor detector and superconductor based transition edge sensors for the detection CEνNS. COHERENT previously have detected the CEνNS using a CsI detector. But MINER will be the first to detect CEνNS from a reactor based neutrino source. It is located in nuclear science center at Texas A & M university, USA. Along with detection of CEνNS, it also aims to detect sterile neutrino oscillation with the help of movable core technology[9].

1.2.1 Experimental set-up

MINER uses 1MW TRIGA (Training, Research, Isotopes, General Atomics) reactor as the neutrino source. Neutrino is released from the beta decay of radioactive daughter nucleii which are produced during the fission process of uranium in the core. The nuclear core is kept inside a pool with cooling system to prevent the nuclear fuel from burning out (Fig.1.2).

Fig:1.2 shows the presence of nuclear core(bright light) inside a pool in MINER.

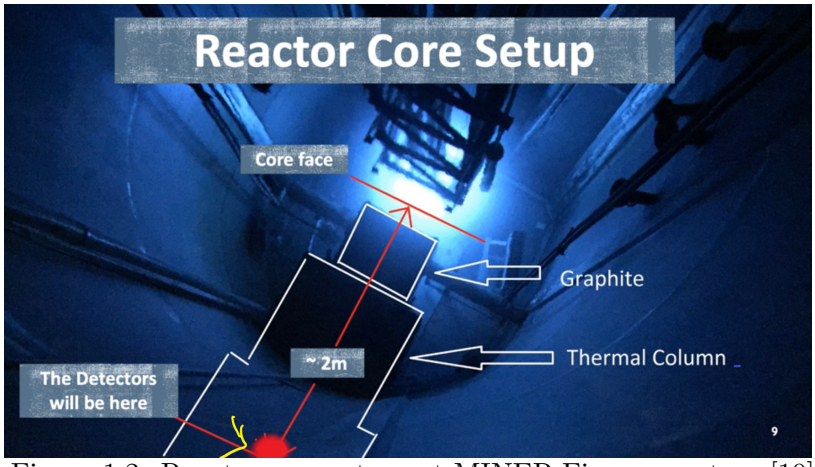

Figure 1.2: Reactor core set-up at MINER.Figure courtesy [10]

The pool is covered with concrete wall to prevent backgrounds like α, β, γ particles and neutrons. Figure also shows a schematic of thermal column within the concrete wall. Graphite kept in between the thermal column and the reactor core. It helps to reduce the energy of the fast neutrons coming from fission such that they can be reusable for the fission process. Detectors are kept inside this thermal column and neutrino releasing from the reactor core reaches here. The key configuration here is movement ability of the reactor core, this enable exposure of the detector from the source at various distances. Observing neutrinos at different distances may help to find the BSM event sterile neutrino oscillation (oscillate between different flavours with distance).

1.2.2 Reactor neutrinos and Expected interaction rate

Neutrino flux in the detector at 2 m from reactor core is calculated to have an rough estimate of number of neutrino detector is facing per unit time. Also by knowing $CE\nu NS$ scattering cross section, we calculate total number of interaction possible for a silicon detector with some given mass e.g.100 gm.

No. of ν from 1MW reactor:

Amount of energy and neutrino released per fission process is calculated in appendix, results are used below.

Average energy released per fission 200 MeV (Appendix-A)

Number of fission in 1MW reactor $=\frac{1MW}{200MeV} = \frac{1}{3.2} \times 10^{17}$ /sec.

Neutrino released per fission is 6 (Appendix-A),

Total ν flux$=\frac{1}{3.2} \times 10^{17} \times 6 = 1.87 \times 10^{17}$.

No of ν Interaction at the detector:

For a silicon detector of mass 100 gm and kept at distance 2 m from the reactor core.

ν flux at 2 m from the reactor$=\frac{\text{Total neutrino flux}}{4\pi r^2} = 3.73 \times 10^{11}/cm^2/sec$

Number of interaction=No. of silicon atom in 100 gm$\times$ Scattering cross section $\times$ ν flux at 2 m.

Number of interaction is found to be 0.488 /day.

So we are expecting 1 neutrino per two days to interact with our detector if our detector is made up of silicon with mass 100 gm.

Chapter 2

Detector working principle

In this section, physical principle for measuring an event by the detector is described. Event is defined when an incoming particle interact with the detector material and some of it's energy is transferred to the detector. Energy is propagated from the interaction site to the sensors of the detector via electrons, photons or collective excitation of the crystal lattice which is also called as phonons. One can see a schematic of energy transfer phenomenon from the point of interaction to the sensors in Fig.2.1. By measuring the signal through the sensor we can analyze about the properties of the interacted particle. This thesis focuses on the experiments which have done using semiconductor detectors, where mode of transmission of energy is basically phonons and electrons. Electron propagation and detection is not included in this thesis, here we will only deal with phonon sensor detectors that I am working with. Unlike semiconductor detector energy transportation occurs through sapphire detector via photons and phonons. Here also the detector measure only phonons. Photons coming from the detector have different purpose which is described in the next chapter.

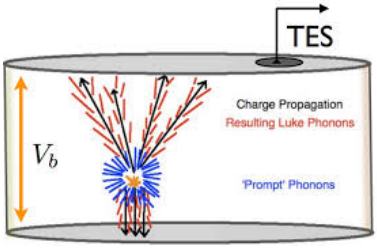

Figure 2.1: Picture of an event occurred inside a detector. Arrows corresponds to electron and blue and red lines correspond to phonon propagation.

This chapter is divided in three sections, (1) Incoming particle interaction with detector material, (2) Phonon propagation in the detector ,and (3) Detection of phonons by the sensors in the detector.

2.1 Particle interaction

When an external particle hits the detector it can interact with either electron or with the nucleus of the detector material. If it hits with electron it is called electron recoil otherwise nuclear recoil. Let's discuss each case briefly.

Electronic recoil:

I am working with silicon semiconductor detector. Silicon has e^-/h^+ pair production energy (E_{e^-/h^+}) 3.6eV and band gap energy (E_{gap}) 0.74eV. Pair production energy is the energy it required to free the electron from the atom and band gap energy is the energy it required to send the electron form the valence band to the conduction band. When the recoil energy of the event is greater than the pair production energy it will produce one e^-/h^+ pair and e^- will retain excess recoil energy as kinetic energy. If possible the excited electron will produce more e^-/h^+ pair in it's surrounding with the excess kinetic energy until the energy falls below the pair production energy. At this point they will not be able to create one more e^-/h^+ pair. So number of e^-/h^+ pair produced for an given recoil energy E_R will be

$$E_R = nE_{e^-/h^+} \tag{2.1}$$

where n is the total number of e^-/h^+ pair produced. Now all the electron will move down to conduction band from it's free electron state ($3.6eV \rightarrow 0.74eV$) and the energy difference will be emitted via phonons in the crystal. This initial phonon that released after an interaction will be called prompt phonons. Energy contained by electrons (E_{e^-}) and phonons (E_{phonon}) after an interaction is found out to be

$$\begin{aligned} E_{e^-} &= nE_{gap} \\ E_{phonon} &= n(E_{e^-/h^+} - E_{gap}) \end{aligned} \tag{2.2}$$

Ionisation yield which is defined as the ratio between ionization energy and phonon

energy will be[11].

$$Y_{ER} = \frac{E_{e^-}}{E_{phonon}} = \frac{E_{gap}}{E_{e^-/h^+} - E_{gap}} \tag{2.3}$$

where Y_{ER} is the ionization yield for electron recoil event.

Nuclear recoil:

In this case nucleus possess the recoil energy after the interaction. Due to kinematically unfavourable condition electron can not share it's energy to nucleus and hence, only share with surrounding electrons. But nucleus having heavier mass side can give energy to electrons as well as surrounding nucleus. Recoil energy given by an external source now distributed among the surrounding electrons and nucleus through one single nucleus. Some of the energy contained by the electrons will be retained by themselves and some will be shared to phonons as described before, but all the energy contained by the nucleus is given to phonons only. So, in the case of nuclear recoil phonon energy is contributed from nucleus and electrons and electron energy is contributed due to electron only. This causes a different ionization yield as compared to the case of electron recoil where contributions to phonon and electron energy are due to electron only. Ionization yield will be different for different materials which will depend on the capability of nucleus share it's energy to other nucleus or electron, it is theoretically derived by Lindhard using condensed matter theory[11].

$$Y_{NR} = \frac{kg(\epsilon)}{1 + kg(\epsilon)} \tag{2.4}$$

where $k = 0.133Z^{2/3}A^{-1/2}$, $g(\epsilon) = 3\epsilon^{0.15} + 0.7\epsilon^{0.6} + \epsilon$ and $\epsilon = 11.5Z^{-7/3}E_{recoil}$, Z-atomic number, A-mass number of the detector material used and E_{recoil} is the nuclear recoil energy. Here ϵ and k relates to stopping power of the nucleus and electrons in the lattice to the moving ions.[12]

Ionization yield is calibrated to 1 for electron recoil. We know that the for the same energy recoil more energy is shared as phonon energy in the nuclear recoil as

compared to the electron recoil. That says that there is less ionization yield for the case of nuclear recoil. Calibrating the Y_{ER} as 1, Lindhard got $Y_{NR} \sim 0.3$ for for silicon and germanium material.

2.2 Phonon propagation

Depending on the location of phonon production there are three types of phonons[13]

1. Prompt phonon: Produced after intial interaction (Blue lines in Fig.2.1).
2. NTL (Neganov-Trofimov-luke) phonon: Produced when electrons move through the crystal (Red lines in Fig.2.1).
3. Recombination phonon: Electrons after reaching the electrode move down from conduction band to valence band and release the energy as phonons.

Prompt phonons:

They are the phonons which are produced at the interaction site as discussed above. Energy contained by them is also discussed which is

$$E_{phonon}^{prompt} = n(E_{e^-/h^+} - E_{gap}) = E_R - nE_{gap} \tag{2.5}$$

Prompt phonons after emitting from the interaction site rapidly move and fill out the whole detector by the process called isotope scattering, where phonons scatter elastically from different isotopes in the crystal lattice [13]. Also phonons scatter in-elastically in the crystal lattice due to higher order anharmonic nature of the crystal lattice. Harmonic potential in the lattice produce stationary states of constant frequency, but due to some deviation from harmonic potential in the lattice phonon frequency or energy decay over time [13]. So phonons move quickly in the crystal that implies it will get detected by the sensors, but as they also decay there is chance of energy loss not measured by the sensors.

NTL phonons:

It is named after three scientist named Neganove, Trofimov and Luke. According to them, when we increase the biasing voltage across the detector, electron will accelerate in the crystal along the electric field produced due to the biasing. But it's movement will be hindered by the electrons and nucleus present in the lattice, so it will attain a constant drift velocity and rest other energy will be emitted as phonons. These phonons will also be emitted in the direction of propagation of the charge carriers. So, phonon energy collected will be energy given to the charge carriers (eV) subtracted to energy kept by the charge carriers (E_{KE})

$$E_{phonon}^{NTL} = neV - nE_{KE} \tag{2.6}$$

Recombination phonons:

Electrons after reaching to the sensors deposit themselves in the electrode and shed all their remaining energy (E_{gap} and E_{KE}) to phonons.

$$E_{phonon}^{Rcomb} = nE_{gap} + nE_{KE} \tag{2.7}$$

Total energy collected by phonon sensors is

$$\begin{aligned} E_{phonon}^{total} =& E_{phonon}^{prompt} + E_{phonon}^{NTL} + E_{phonon}^{Rcomb} \\ =& E_R - nE_{gap} + neV - nE_{KE} + nE_{gap} + nE_{KE} \\ =& E_R + neV \end{aligned} \tag{2.8}$$

2.3 Phonon detection

After reaching the sensors there are two mechanisms left which lead to the detection of the signal by oscilloscope. Firstly phonons collection mechanism at the sensors and secondly, conversion of these phonon energy to electric signal.

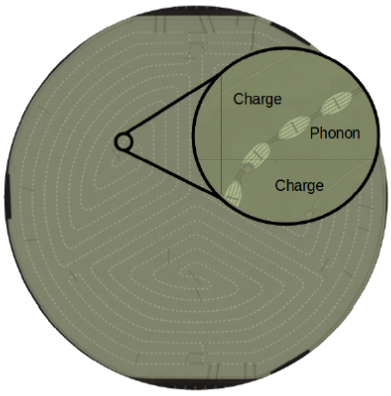

(a) Top view

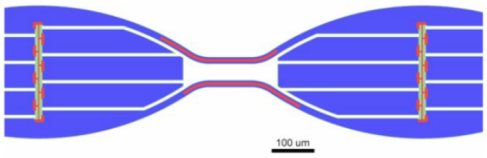

(b) Al fin(blue), W(red)

Figure 2.2: Top view of detector with sensors[14]

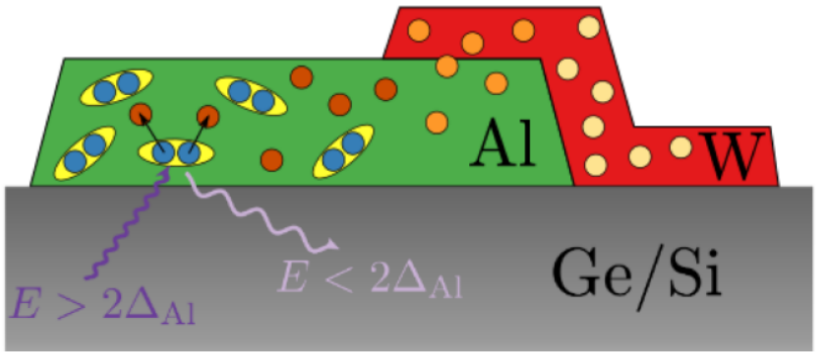

Figure 2.3: Phonon collection at TES[14]

2.3.1 Phonon collection at TES (transition edge sensors)

Figure 2.2a shows the top view of the detector where TES (transition edge sensors) are chained to form different channels. Figure 2.2b shows the zoomed version of each sensor where the blue part is aluminium fin, red part is tungsten filament. Figure 2.3 shows side view of the detector having Ge/Si material in it's bottom, and Al, W are kept on the top surface act as sensors. Aluminium is kept below the transition temperature, so electrons inside it are bound as cooper pairs. Phonons after reaching to the aluminium surface break these cooper pairs and make free electrons. These electrons will now move to tungsten system and break the cooper pairs there to form

free electrons.

Increase in free electron in W filament increase it's resistance drastically as due to the process W cross the transition temperature. W was previously biased at some constant voltage by an external source, so increase in resistance causes decrease in power supply through the W filament (as $P \propto \frac{V^2}{R}$). Decrease in power supply accompany with decrease in heat through the system , hence, system cools down and W falls below the transition temperature. W is now ready for interaction with another phonon. This mechanism is called electro-thermal feedback. Mathematical description heat fall time is given in the following paragraph [14].

Initially without any phonon involvement in the sensors, only heating source was power supply due to external biasing voltage on W filament and cooling source was the refrigerator where the system is kept. So the heat change equation is written as

$$c_v \frac{dT}{dt} = \frac{V_b^2}{R(T)} - \kappa(T^5 - T_s^5) \tag{2.9}$$

c_v=Heat capacity of W, κ=Thermal conductivity, V_b=Voltage bias across W, T_s= Temperature of the source(refrigerator), T= Temperature in W material. First term in RHS shows joule heating that causes increase in heat or temperature while second term shows decrease in temperature due to cooling effect of refrigerator.

At equilibrium LHS=0, but a small change in temperature will vary in the system following above equation. Let the temperature changed by amount $T = \delta T$ due to phonon effect. Then

$$\begin{aligned} c_v \frac{d(T+\delta T)}{dt} &= \frac{V_b^2}{R(T+\delta T)} - \kappa((T+\delta T)^5 - T_s^5) \\ &= \frac{V_b^2}{R(T) + \frac{dR}{dT}\delta T} - \kappa(T^5(1+\frac{\delta T}{T})^5 - T_s^5) \\ &= \frac{V_b^2}{R(T)}(1 - \frac{1}{R}\frac{dR}{dT}\delta T) - \kappa(T^5 - T_s^5) - 5\kappa T^4 \delta T \\ \Rightarrow c_v \frac{d(\delta T)}{dt} &= -\frac{1}{c_v}(\frac{V_b^2}{R^2(T)}\frac{dR}{dT} + 5\kappa T^4)\delta T \end{aligned}$$

$$\delta T(t) = \delta T(0) \exp -\frac{1}{c_v}(\frac{V_b^2}{R^2(T)}\frac{dR}{dT} + 5\kappa T^4)t$$
$$\delta T(t) = \delta T(0) \exp \frac{-t}{\tau} \tag{2.10}$$

Here half life decay $\tau = \frac{c_v}{\frac{V_b^2}{R^2(T)}\frac{dR}{dT}+5\kappa T^4}$ is the fall time of a pulse and can be calculated by putting the appropriate parameters.

As shown in Fig.2.2a nearly 400-500 TES are kept connected inside one channel of the detector. Likewise four such channels are made as shown in the figure. Each channel combines all the contribution from it's TES and connect to an external circuit through a wire. So the channels take the reading of an event instead of each TES and we will record the data through each channel.

2.3.2 Conversion of change in temperature to electronic signal

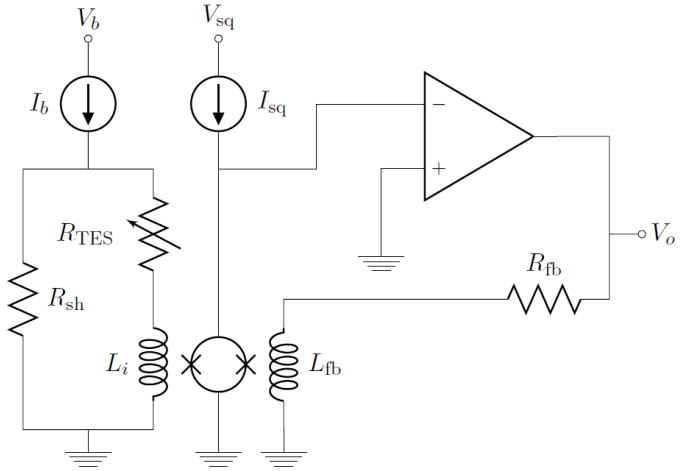

Figure 2.4: Phonon channel readout circuit.[14]

Above figure shows the electronic circuit that connects TES to Op-Amp (operational amplifier) and finally op-amp shows the output voltage. Left loop of the figure shows that the decrease in temperature across TES causes increase in resistance, hence decrease in current and decrease in magnetic flux by the left inductor. This change in the magnetic flux is compensated by the inductor in the right loop when

appropriate current is provided by the op-amp [14]. For change ion current I_i in the left loop, the current produce in the right loop will be depend on the equation

$$L_i I_i = L_{fb} I_{fb} \tag{2.11}$$

L_i, L_{fb}=Inductance in left and right loop respectively. I_i=Decrease in current through TES. I_{fb}=Current from op-amp and

$$\begin{aligned} V_0 &= I_{fb} R_{fb} \\ V_0 &= \frac{L_i R_{fb}}{L_{fb}} I_i \end{aligned} \tag{2.12}$$

where V_0 is the output voltage. We here see that output voltage is directly related to change in current from TES. Which in turn is connected to the change in temperature and hence to initial interaction. So we will get a pulse from initial interaction.

Chapter 3

Detectors at MINER

Texas A & M university, USA is setting up an experiment called MINER (Mitchell institute of science education and research) to detect rare event like $CE\nu NS$. Before starting the science run, several engineering runs are performed using different kinds of detectors in different set-ups for (1) better understanding of backgrounds and rejecting them, (2) observing the efficiency of the detectors for the detection of low energy recoil. In this thesis properties of the silicon high voltage detector (SiHV), hybrid detector and sapphire detector have been analyzed. Properties of SiHV include (i) low energy detection via increasing biasing voltage (ii) increasing energy resolution with increase in biasing voltage, properties of hybrid detector includes (i) Both low energy detection and increase in energy resolution with increase in biasing voltage (ii) electron recoil (ER) and nuclear recoil (NR) discrimination, and sapphire detector include (i) lowering of energy resolution compared to both the silicon based detectors. These detectors differ from each other by their shape as well as core material used. Experiments have been performed by using these detectors in different voltage bias, exposing them with different radioactive source and with some additional changes like temperature. All have been used in cryogenic (low temperature) environment to detect low energy signal.

Basic properties of these three detectors have been emphasized in the first part of this chapter, second part of the chapter contains information related to the external environment in which the detectors are kept.

3.1 Detectors

3.1.1 Silicon high voltage detector (SiHV)

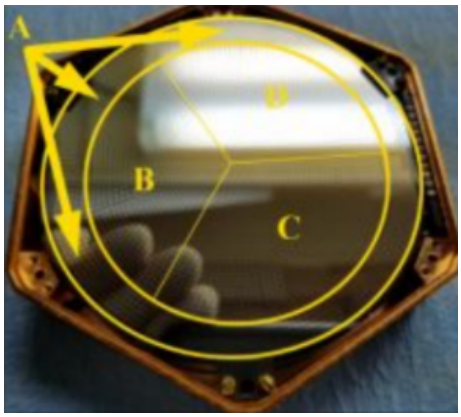

Figure 3.1: Bottom surface of SiHV detector. Plot labels 4 phonon channels A, B, C and D on it.

- Made up of ^{28}Si substrate.
- It is a cylindrical detector with diameter 7.5cm , height 1cm and mass 100gm.
- It consists of sensors which detects only phonon signal.
- It is having 4 phonon channels which include 3 inner channel B, C, D and one outer ring channel A as shown in Fig.3.1.
- Biasing is given to the bottom surface.

The major advantage by the use of this detector is the high voltage biased. The high voltage biased helps in the detection of very low recoil energy through the effect of NTL gain (Section.2.1). But due to this high voltage biasing, there is a chance of increase in amplitude of noise signals (electronic noise) also which would increase a similar manner like low energy signal and hinder the process of detection. However, presence of phonon only sensors solves this issue, noise does not get amplify with increasing biasing voltage while measuring through phonon signals only[15]. It would not be the case if a detector with charge sensors is used. For this reason a phonon sensor based detector is used for the detection of low energy signal.

Both the properties that are expected to observe by the use of this detectors have been analyzed with the use of data in the next chapter of this thesis. However, this detector is not well enough to distinguish a major background in the process of $CE\nu NS$ detection. That is electron recoil. A new silicon based detector with unique shape has been built for better discrimination of this particular electron recoil

background. The detector is called hybrid detector is also described in this thesis.

3.1.2 Hybrid detector

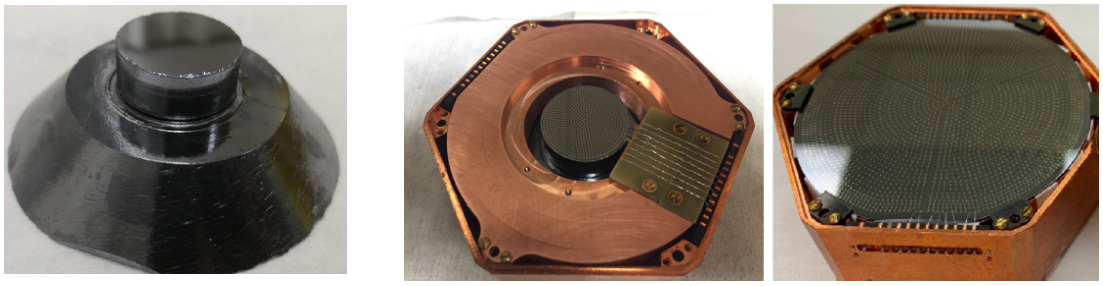

Figure 3.2: Figure of hybrid detector (left), top surface of the detector having one channel (middle), Bottom surface having 4 channels same as described in case of SiHV (right)

- Made up of ^{28}Si substrate.
- It is made by cutting a cylindrical detector into the weird shape as shown in the left plot of Fig.3.2. It has bottom part of diameter 7.6cm, top part with diameter 2.5cm and height 2.5cm. The side surface is carved at an angle 45°.
- Like SiHV, it also consists of sensors which detects only phonon signal.
- It has 4 phonon channels at the bottom part of the detector which include 3 inner channel B, C, D and one outer ring channel A. Apart from the bottom part it also has one channel at the top surface.
- Biasing voltage is given to the top surface.

To better discriminate between ER and NR hybrid detectors is used. It uses the ionization yield principle for this distinction (Section.2.1). According to the principle ionization yield will be higher in ER compared to NR. But to calculate ionization yield we need to measure both the energy given to charge carriers or ionization energy and energy given to the phonons at the site of interaction. Measuring the ionization energy and phonon energy with the help of phonon only sensors is a difficult task. For

SiHV high voltage bias completely mask the initial phonons, and he phonon energy collected is equivalent to the ionization energy.

Hybrid detector is designed to measure both ionization and phonon energy. This is done by the unique shape it possess. Fig.3.3 shows the distribution of the field lines when an external voltage bias is applied. The dense field lines in the top part suggest that charge carriers can accelerate only when they are in this region. Hence NTL phonons will be created in the top part only. As bottom part being the bulk of the detector, most interaction occur there only. After the interaction phonons will not able to pass to the top part due to very narrow opening to the top part, they will reflect and stay in the bottom part until get absorbed in the bottom channel. And electrons move to the top part following the field lines also there they produce NTL phonons and they get collected in the top part. This phonon is related to ionization. In this way initial phonon energy get collected at bottom channel and ionization energy get collected at the top part of the detector. So ionization yield is calculated by dividing the energy detected in the top and bottom part of the detector.

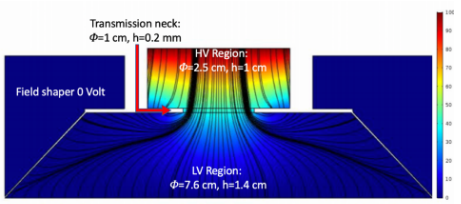

Figure 3.3: Electric field lines when voltage is biased in the detector. Due to the configuration strong field lines observed in the top part of the detector.[15]

Along with this advantage, it also has capability to detect low energy signal (NTL gain) like SiHV, So we want to test it's NTL gain property as well as test the growth of noise at higher voltages.

3.1.3 Sapphire detector

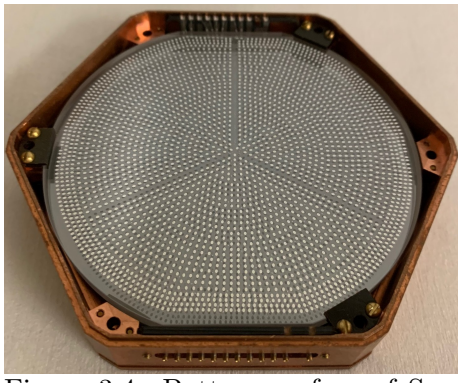

Figure 3.4: Bottom surface of Sapphire detector. similar configuration like SiHV detector and Hybrid detector bottom surface.

- Made up of Al_2O_3 substrate.
- It is a cylindrical detector with diameter 7.5cm , height 0.4cm and mass 73gm.
- It consists of sensors which detects only phonon signal.
- It is having 4 phonon channels (3 inner channel named B, C, D and one outer ring channel A).

Energy is transported in sapphire detector by photons and phonons. Here energy transportation is different from the case of silicon detectors that we studied. Sapphire is made up of aluminium substrate Al_2O_3. And we have discussed in the previous chapter that Al fins are kept over detector for absorption of phonons from the detector material to the sensor. Here due to transport of phonons from Al to Al only efficiency of transportation of phonons will be higher.

Here production phonons comes with the production of photons, which is different from the perspective of semiconductor detectors. With different production mechanism baseline resolution is expected to get smaller and discussed with proper analysis in next chapter.

Experiments with the detectors are generally done by stacking two (other one is SiHV used generally) detectors and measuring the events. Photons are produced in response to any interaction with the sapphire material, and those photons can be traced using another detector which is stacked over sapphire detector. So, one event can be detected by two detector, correlation plot is plotted between the energy measured by the two detector and is described in the next chapter.

3.2 Experimental set-up

Figure.3.5 shows the experimental set-up for the experiments that are performed to test the detectors properties. As we need to work at extreme low temperature regime for proper working of superconductor material which acts as sensors, detectors are kept inside a $^3He - ^4He$ dilution refrigerator. Proper biasing is also given across the two ends of the detector for low energy detection.

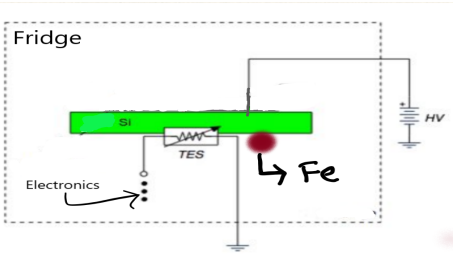

Figure 3.5: Schematic of experimental setup conducted at MINER.

TES associated different channels of the detector are connected with the electronic circuit and then to oscilloscope to observe the signal as explained in subsection.2.3.2. In this particular experiment as shown in Fig.3.5, ^{52}Fe is kept over SiHV as a known γ source for testing detector properties. Wires collected from the above set-up is connected to an oscilloscope directly or through a 14-bit digitizer. So data came in the units of voltage or ADC (analogue to digital converter) units.

Different sources like ^{52}Fe, ^{241}Am and ^{252}Cf are used as known γ or neutron sources in different experiments.

Source name	Emitted particle	Known peaks	Probable interaction
^{52}Fe	photon	5.89keV	ER
^{241}Am	photon	13.9keV and 59.54keV	ER
^{252}Cf	photon	No peak	ER
	neutron	No peak	NR

Table 3.1: Sources with their emitted particle and known emission peaks.

Chapter 4

Detector data analysis

In this chapter data analysis from each of the three detectors is shown in separate sections. Different properties of the detectors along with some analysis techniques are discussed in the following sections. First section is written on silicon high voltage detector (SiHV) which include (i) energy calibration using a known γ source, (ii) observing NTL gain which confirms the detection of low energy recoil, (iii) partition plot to identify the location of the source and (iv) baseline resolution to confirm noise does not get amplify with increase in biasing voltage. second section is written on hybrid detector which include (i) energy calibration, (ii) observing NTL gain, (iii) partition plot, (iv) baseline resolution, and (v) electron recoil (ER) and nuclear recoil discrimination (NR) plot which suggest better background rejecting capability of this detector. Last and third section of this chapter includes (i) energy calibration, (ii) correlation plot of sapphire detector with SiHV detector (3.1.3), and baseline resolution of the detector. Different properties were verified by experiments using these detectors. Data analysis is done using PYTHON language by the use of NumPy[16], SciPy[17], QETPy[18], MatPlotLib[19] software.

4.1 Silicon high voltage detector (SiHV)

Data given reflects from the experiment using SiHV which is done at TAMU on 19 July, 2020. This Data is analyzed and shown in different subsections. This section is proceeded as follows: information about the data $\rightarrow$ energy calibration using data $\rightarrow$ NTL gain (low energy detection) $\rightarrow$ Baseline resolution (to observe noise at increasing

Voltage(V)	No. of Pulses	No. of Noise pulses
0	29866	1006
50	31005	1236
100	34354	1063
150	30368	1038
200	30069	1094
250	32311	4554

Table 4.1: High voltage dataset.

biasing voltage) → Partition plots (to find location of the source). Figure.3.5 depict the set-up for this particular experiment. Just like the figure, detector is kept inside a fridge with ^{55}Fe source kept at bottom surface of the detector (same side of the phonon sensors) .

Table.4.1 shows the number of pulse and noise samples recorded at different biasing voltage for the experiment. Pulse samples are taken by putting a trigger condition on pulse amplitude and noise samples are taken by putting random trigger condition without any preference for amplitude. 14-bit digitizer converts voltage to ADC unit and output is provided with the help of an oscilloscope. Figure.4.1 shows ^{55}Fe pulse sample and noise sample at biasing voltage 50V. Pulse or noise sample is collected for 2.56 ms and each sample contains 2000 data point with 1.28 μs data point spacing. Using the information from data we try to compute the energy contained in it and observe the properties explained in subsection.3.1.1.

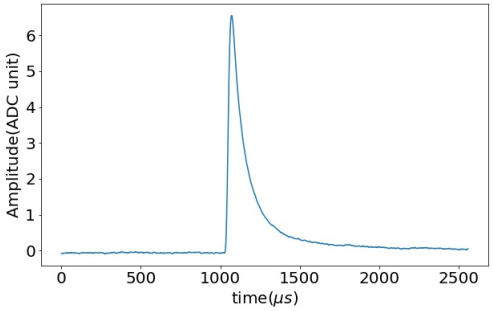

(a) ^{55}Fe pulse sample

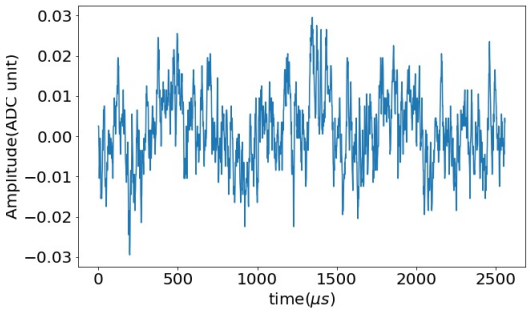

(b) Noise sample

Figure 4.1: Detector signal.

4.1.1 Energy Calibration

We use two ways to calculate energy contained by the pulse. First way (Pulse integral method) is integrating pulse region and the second way (Optimal filter method) is fitting the pulse and taking the peak of the fitted pulse as measure of energy. Both ways are described briefly with their subsequent plots.

Pulse integral method

If A(t)=Amplitude of the pulse at different time and t=time of points being taken then pulse integral can be calculated as follows.

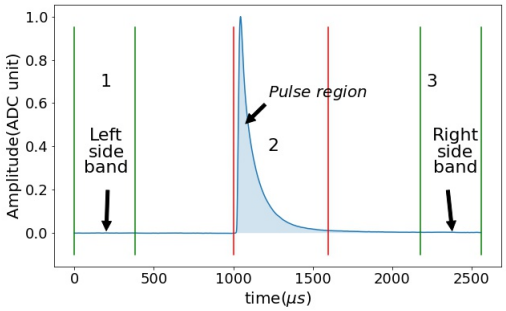

Figure 4.2: Pulse integral method

- Integrate the region containing pulse (region-2)

$$I = \int_2 A(t)dt$$

- Now integrate the side regions to know average noise contained in the pulse trace.

$$N = \frac{\frac{\int_1 A(t)dt}{\int_1 dt} + \frac{\int_3 A(t)dt}{\int_3 dt}}{2}$$

- Subtracting noise from signal we get the energy contained by the pulse only. So pulse integral will be

$$PI = I - \int_2 N dt \tag{4.1}$$

- Energy from each channel is added to get the final value for total bottom channels. Total energy contained by the bottom channel will be

$$PI^{HV}_{bottom} = PI_B + PI_C + PI_D, \text{ For Si HV} \tag{4.2}$$

Looking through all the pulse samples Region-1 and Region-3 are chosen to be of length $300\mu s$ and Region-2 of length $600\mu s$.

Pulse integral value is calculated for each pulse using above procedures, all the values were then plotted in a single histogram plot to know the energy spectrum computed by the detector for ^{55}Fe. Plot is then fitted and calibrated at 5.89keV . Error in the measurement of mean (μ_{err}) can be calculated by

$$\mu_{err} = \frac{\sigma}{\sqrt{N}} \tag{4.3}$$

Where σ is the standard deviation of the gaussian fit to the above energy spectrum and N is the number of data points contained in the gaussian fit.

Looking into different plots it is observed that energy contained by the pulse is increasing with increase in biasing voltage. It is also seen that at zero voltage biased detector is not well enough to identify the ^{55}Fe signal over the noise. So rest of the study is done only at high biasing voltage.

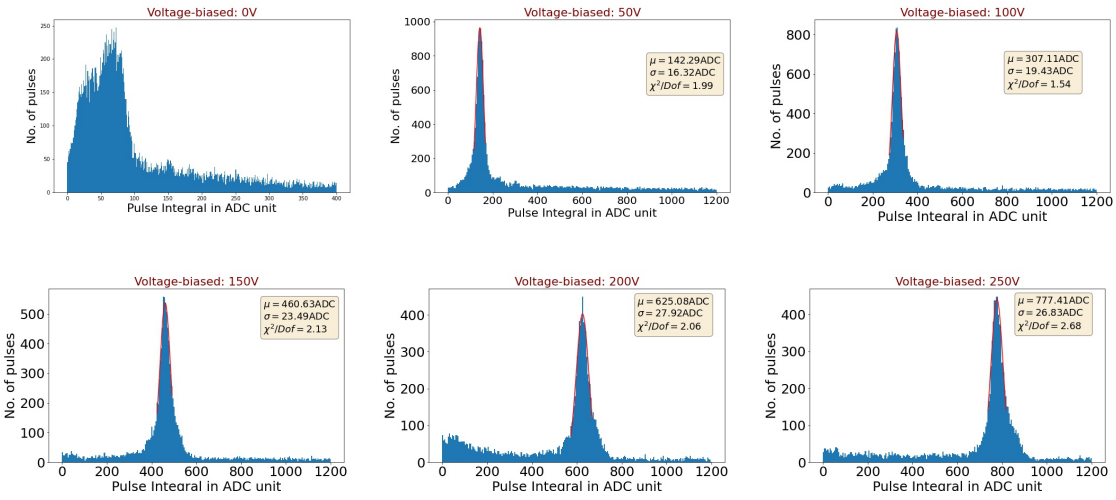

Figure 4.3: Energy spectrum of ^{55}Fe using SiHV detector for different biasing voltage. Energy calculated using pulse integral method.

Optimal Filter method

Another method to findout the energy content of the pulse. It fits the pulse with an expected pulse known as pulse template and amplitude of the fit is considered to be the energy of the pulse. Pulse template is made by averaging all pulse traces, the idea is to cancel all the fluctuations by averaging over all the pulses which eventually should give an pure estimate of the pulse. A general pulse is said to be combination of known pulse and noise by the following relation[20]

$$S(t) = aA(t) + n(t) \tag{4.4}$$

Where S(t) is the observed Signal, A(t) is the normalized pulse template, n(t) is noise and a is the scaling factor or the amplitude of the fit. Now a is found out by fitting through χ^2 minimization method.

$$\chi^2 = \frac{\int (S(t) - aA(t))^2 dt}{\sigma^2} \tag{4.5}$$

Where $\sigma^2 =< n(t)^2 >_t = \frac{\int (n(t))^2 dt}{\int dt}$. For physical noise it is assumed that different terms of noise have no correlations in frequency space, so we move into frequency space by fourier transform for ease of calculation[20]. In fourier space Eq:4.5 will be converted to

$$\chi^2 = \frac{\int |\tilde{S}(\nu) - a\tilde{A}(\nu)|^2 d\nu}{\int J(\nu) d\nu} \text{ where } J(\nu) = |\tilde{n}(\nu)|^2/T \tag{4.6}$$

Value of a is found out by using the relation $\frac{\partial \chi^2}{\partial a} = 0$, so the value of a at minimum χ^2 is found out to be

$$a^* = \frac{\int \frac{\tilde{A}^*(\nu)\tilde{S}(\nu)}{J(\nu)} d\nu}{\int \frac{|\tilde{A}(\nu)|^2}{J(\nu)} d\nu} = \frac{\int \phi^*(\nu)\tilde{S}(\nu) d\nu}{\int \phi^*(\nu)\tilde{A}(\nu) d\nu} \text{ where } \phi^*(\nu) = \frac{\tilde{A}^*(\nu)}{J(\nu)} \tag{4.7}$$

Here $\phi(\nu)$ is used as a filter which selects some frequency of the signal and rejects some frequency. This selection technique of $\phi(\nu)$ name this process as optimal filter.

Optimal filter with time offset

If certain signal has start time (time at which pulse reaches 10% of it's maximum amplitude) like Fig.4.4 such that it is not matching with the template start time, then the χ^2 minimization method should also consider the delay time into calculation. Then any pulse can be written as the equation[20]

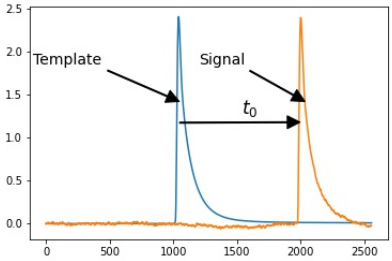

Figure 4.4: Optimal filter with time offset

$$S(t) = aA(t - t_0) + n(t) \tag{4.8}$$

χ^2 for this case in fourier space is found to be

$$\chi^2 = \frac{\int |\tilde{S}(\nu) - ae^{-i\nu t_0}\tilde{A}(\nu)|^2 d\nu}{\int |J(\nu)|^2 d\nu} \tag{4.9}$$

By putting $\frac{\partial \chi^2}{\partial a} = 0$, it gives

$$a^* = \frac{\int e^{i\nu t_0} \frac{\tilde{A}^*(\nu)\tilde{S}(\nu)}{J(\nu)} d\nu}{\int \frac{|\tilde{A}(\nu)|^2}{J(\nu)} d\nu} = \frac{\int \phi^*(\nu)\tilde{S}(\nu)e^{i\nu t_0} d\nu}{\int \phi^*(\nu)\tilde{A}(\nu) d\nu} \tag{4.10}$$

Now for different value of t_0 we have different a, we should consider that t_0 for which χ^2 is minimized. Putting the value of a^* in Eq.4.9 we see that

$$\chi^2_{a^*} = \int \{\frac{|\tilde{S}(\nu)|^2}{J(\nu)} - (a^*(t_0))^2 \frac{|\tilde{A}(\nu)|^2}{J(\nu)}\} d\nu \tag{4.11}$$

From above relation it is clear that χ^2 will be minimum when $a(t_0)$ is maximum. So, the delay time t_0 which gives maximum amplitude in Eq.4.10 will be the best fit to the pulse. Amplitude and χ^2 of the fit is then noted for the particular t_0. The three fit parameter a, t_0, χ^2 are well determined now.

Above three parameters were found computationally using QETPy package of python language. *OF.amp_withdelay* function inside the package takes input as pulse, pulse template and power spectral density of the noise (Appendix-B) and provide output as a, t_0, χ^2. a is taken as the measure of energy and histogram is plotted after

finding a for all pulses. Here some plots is shown for energy measurement at different biasing voltage of the detector.

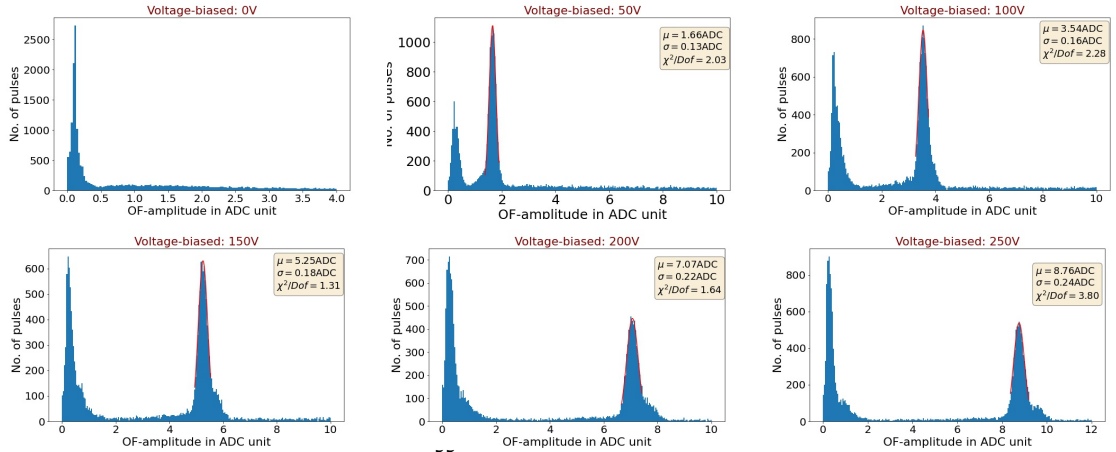

Figure 4.5: Energy spectrum of ^{55}Fe using SiHV detector for different biasing voltage. Energy calculated using optimal filter method.

First peak in the spectrum corresponds to noise signal that comes in the pulse samples. Second peak is the signal coming from ^{55}Fe which also shows shifting in position with increase in biasing voltage. Shifting in position is the fact that energy measured is increasing at increasing biasing voltage which is due to NTL gain effect causing more NTL phonons to reach the sensors. The effect is described by more analysis in the above section.

4.1.2 NTL gain

When we increase the biasing voltage across the detector, NTL phonon production also increases. We can verify this theory using experiments also. We take data at different biasing voltage and observe change in energy with change in voltage. Measurement of energy for this analysis is done using both the methods: pulse integral and optimal filter method.

Pulse integral method:

Figure.4.6 shows ^{55}Fe energy spectrum using pulse integral method in the left and

position of the peak versus biasing voltage is shown in the right. Standard error to for the measurement of peak energy is calculated from Eq.4.3 and also manifested in the right plot. As expected from Eq.2.8 linear gain is observed at increasing biasing voltage (Fig.4.6b).

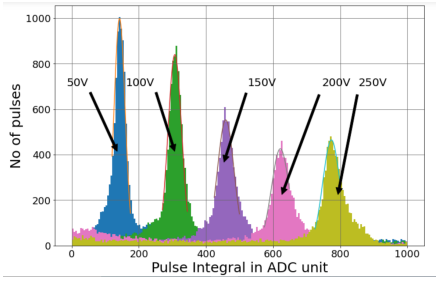

(a) Pulse integral plots

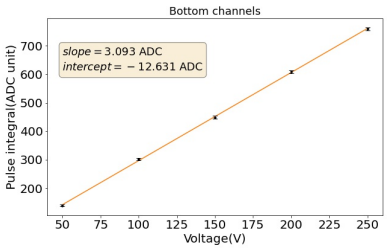

(b) NTL gain

Figure 4.6: NTL gain is shown in both the plots using pulse integral method. Left plots shows the energy spectrum is shifting with increasing biasing voltage. Right plot shows the position shift is linear.

Optimal filter method:

Above result about the detector performance is also confirmed through the optimal filter method. Position of the peak is plotted against biasing voltage. Error bar to the mean is calculated using Eq.4.3 and manifested in Fig.4.7b. Linear gain is verified using optimal filter method also.

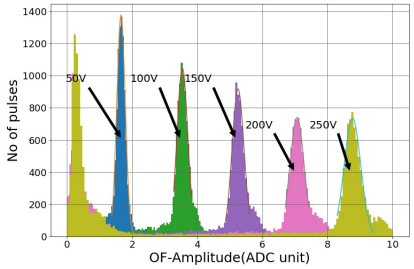

(a) Pulse integral plots

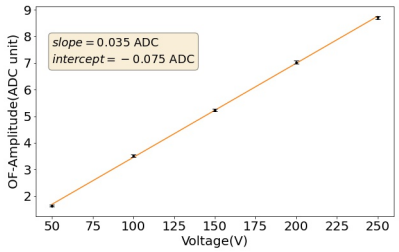

(b) NTL gain

Figure 4.7: NTL gain is shown in both the plots using optimal filter method. Left plots shows the energy spectrum is shifting with increasing biasing voltage. Right plot shows the position shift is linear.

4.1.3 Partition plots

It is an essential technique to figure out the location of source using only the energy content of the pulse. Position of the source is located using the information from all the three channels.

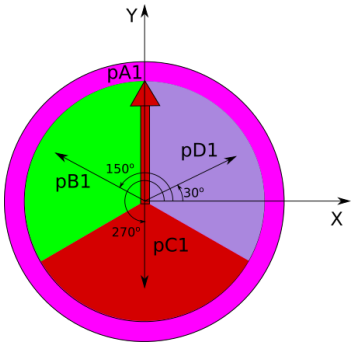

Figure 4.8: Detector configuration

More closer the interaction to any of the channel, more will be the phonon energy deposition in that channel. On this basis of energy deposition in different channels, we can roughly identify the location of the interaction. With the help of configuration of different channels (Fig.4.8), an equation is proposed to identify the X-Y location of the source.

$$
\begin{aligned}
X &= \frac{D_{OF}\cos 30^\circ + B_{OF}\cos 150^\circ + C_{OF}\cos 270^\circ}{B_{OF} + C_{OF} + D_{OF}} \\
Y &= \frac{D_{OF}\sin 30^\circ + B_{OF}\sin 150^\circ + C_{OF}\sin 270^\circ}{B_{OF} + C_{OF} + D_{OF}}
\end{aligned}
\tag{4.12}
$$

where D_{OF} , C_{OF} and B_{OF} are OF amplitude of the pulse in D,C and B channel respectively.

X and Y coordinate for each event is calculated as using Eq.4.12 and are plotted.

Above figure shows a bright spot near the center towards D channel. Brighter spot represents the position of the source. As more interaction is expected to happen in the locality of the source, that put most of the X-Y scatter points around a specific region, hence, a brighter spot. That says that source is kept near the center towards D channel for each biasing voltage while performing the experiment. However, Z component of the interaction can not be determined using this method.

Analysis have done using energy content of the pulse. Now noise effect on the detector should be checked. Next section comprises of resolution of the detector due

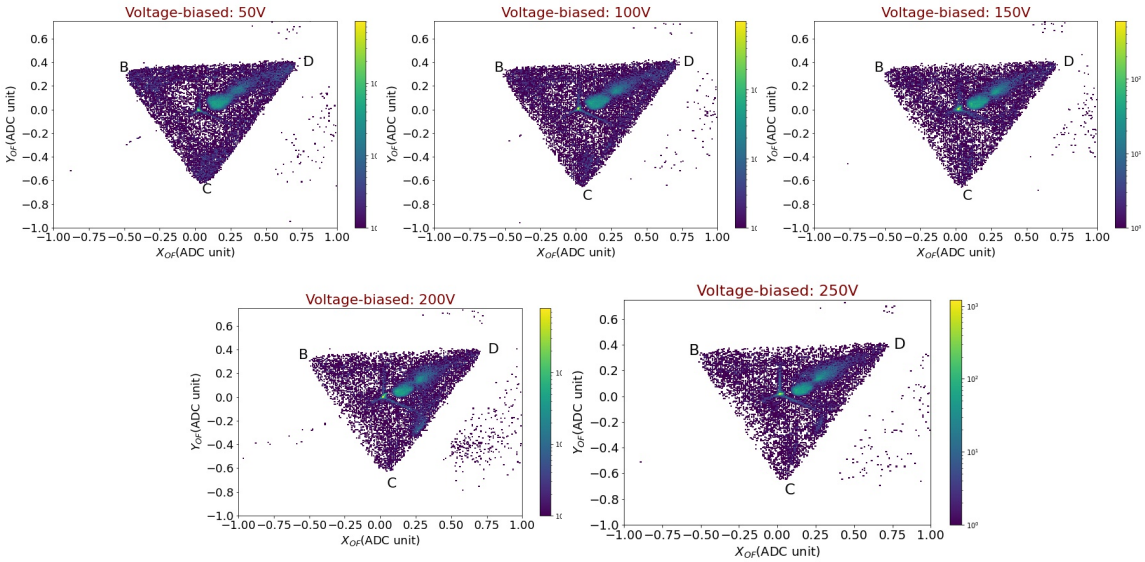

Figure 4.9: Partition plot for different biasing voltage dataset

to presence of noise.

4.1.4 Baseline resolution

Resolution is the minimum difference at which two signals are resolved by the detector. For measurement of energy there are many factors that contribute to resolution. One factor is energy dependent factor, according to it resolution for the peak depends on the energy at which you detect the signal, other is energy independent factor which says that resolution to the peak is independent of the value of the energy. Later type of factor imply that resolution in energy comes due to the noise which is same over all the energy spectrum. This energy independent contribution of noise, influences baseline resolution. More the noise more the baseline resolution and less efficient is the device for detection. Procedure for calculation of baseline resolution

- Find-out the calibration factor by fitting energy spectrum of ^{55}Fe calculated using optimal filter method.
- Do the optimal filter analysis of noise samples and find optimal filter amplitude

for each of the samples.

- Convert the amplitude in KeV scale by multiplying the calibration factor.
- Plot this amplitudes in a histogram and standard deviation of the fit will be the baseline resolution.

Following above procedure baseline resolution for each biasing voltage is calculated and the corresponding energy spectrum of noise is plotted in Fig.4.10. Looking at the value of the resolution this has been found that resolution is decreasing with increasing biasing voltage.

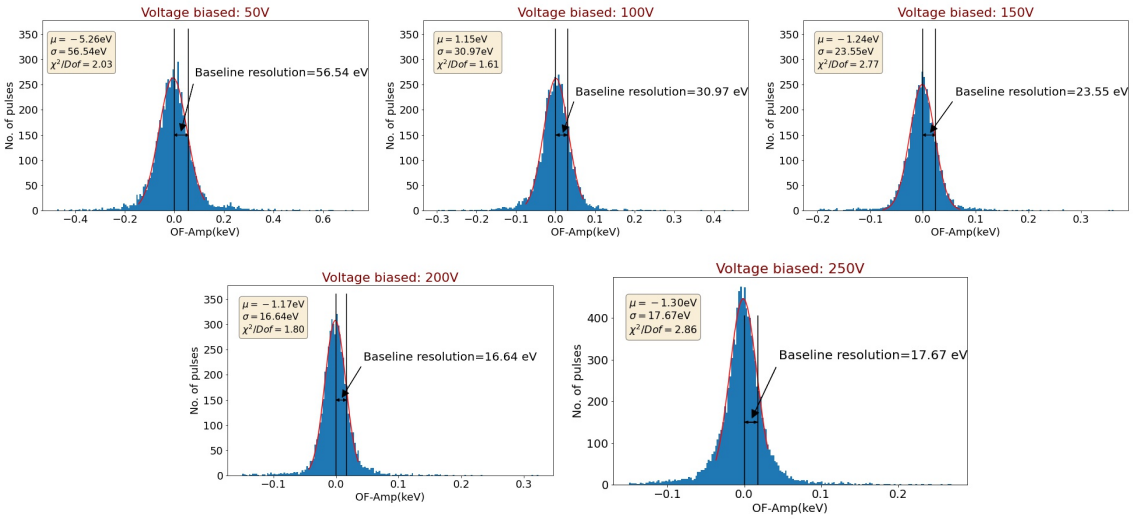

Figure 4.10: Baseline resolution for different biasing voltage dataset

The declination of baseline resolution value with voltage can be described by taking a simple assumption. Baseline resolution is computed by multiplying standard deviation of noise in ADC unit with the calibration factor.

$$\begin{aligned} BR &= \text{Standard deviation of noise in ADC} * \text{Calibration factor} \\ &= \text{Standard deviation of noise in ADC} * \frac{5.89\text{keV}}{\text{peak of the } {}^{55}Fe \text{ in ADC}} \end{aligned} \tag{4.13}$$

where BR is baseline resolution value. Calibration factor contains peak of ^{55}Fe and as we have seen from NTL gain peak increases with increase in voltage. So, the main

hypothesis of this assumption is that peak of the pulse increases with biasing voltage, producing NTL gain energy (2.8) in the denominator, whereas, noise component in the numerator does not vary much except the addition of small parameter called leakage current. As one can see numerator of Eq.4.14 contain N_0 which is the noise at zero voltage biasing and another term is due to the leakage current proportional to biasing voltage V.

$$BR = 5.89 \times \frac{\sqrt{N_0^2 + (Vb)^2}}{E_R + NeV} \tag{4.14}$$

b is leakage current parameter, V is the biasing voltage and denominator is due to NTL gain (Section.2.1).

To prove the correctness of this assumption, this equation is fitted with experimental observation of the baseline resolution value with voltage. And, this fits well to the observed plot (Fig.4.11). That implies with increase in voltage, resolution decreases. According to the model noise remains same with small increase due to the leakage current and energy increases with increase in voltage. So at higher voltage it is a suitable detector to measure energy as noise component does not hinder the process of energy measurement. So high voltage detector is suitable to detect low energy recoil using high biasing voltage.

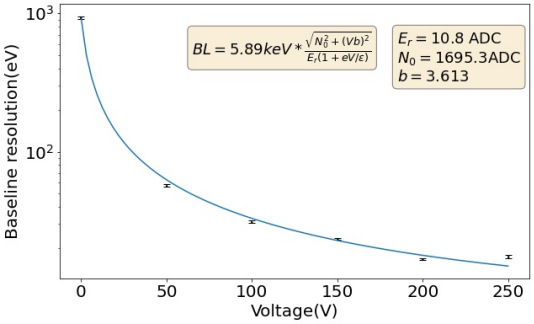

Figure 4.11: Baseline resolution vs voltage in SiHV

4.2 Hybrid detector

As explained in subsection.3.1.2, hybrid detector is built to perform ER and NR discrimination in addition to the performance that SiHV shows. Properties similar to SiHV like NTL gain and Baseline noise resolution is tested and confirmed using one experiment and ER NR discrimination is also tested using another experiment.

Experiment showing similar properties to SiHV is done using hybrid detector at TAMU on 25th October, 2020. Here ^{241}Am is kept as γ source in top surface of the hybrid detector whereas no source is kept at the bottom surface. The configuration of the experiment is kept like fig.3.5. In this experiment data is recorded using all 5

Voltage(V)	No. of Pulses	No. of Noise pulses
8	103381	9709
9	101497	10249
10	110961	12213
12	113889	10103
14	100706	10223
16	100753	15284
18	100902	10502

Table 4.2: Hybrid dataset.

channels: top, A,B,C and D channel rather than 3 used for the case of SiHV. Table.4.2 contains number of pulse and noise samples recorded in each five channels.

4.2.1 Energy calibration

Energy contained in the pulse is calculated using both pulse integral method and optimal filter method. Then it is is calibrated at 59.54keV (known peak for ^{241}Am).

Pulse integral method

In this section energy is calculated using pulse integral method.

Spectrum from bottom channel

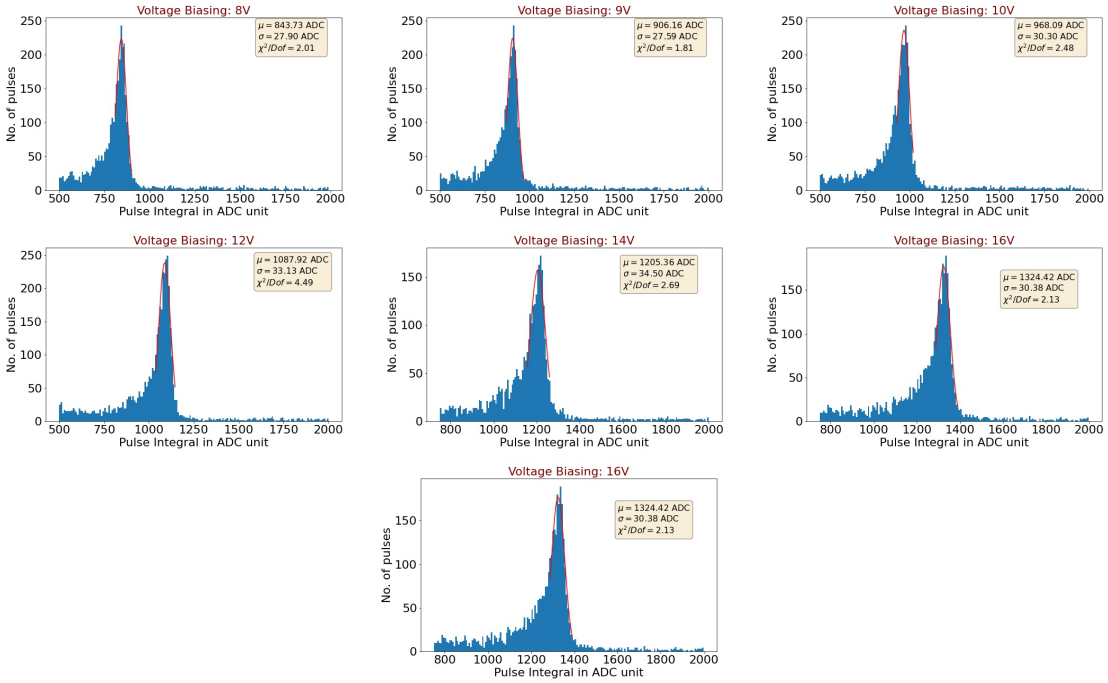

Figure 4.12: Energy spectrum from hybrid detector bottom channels for different biasing voltages

Spectrum from top channel

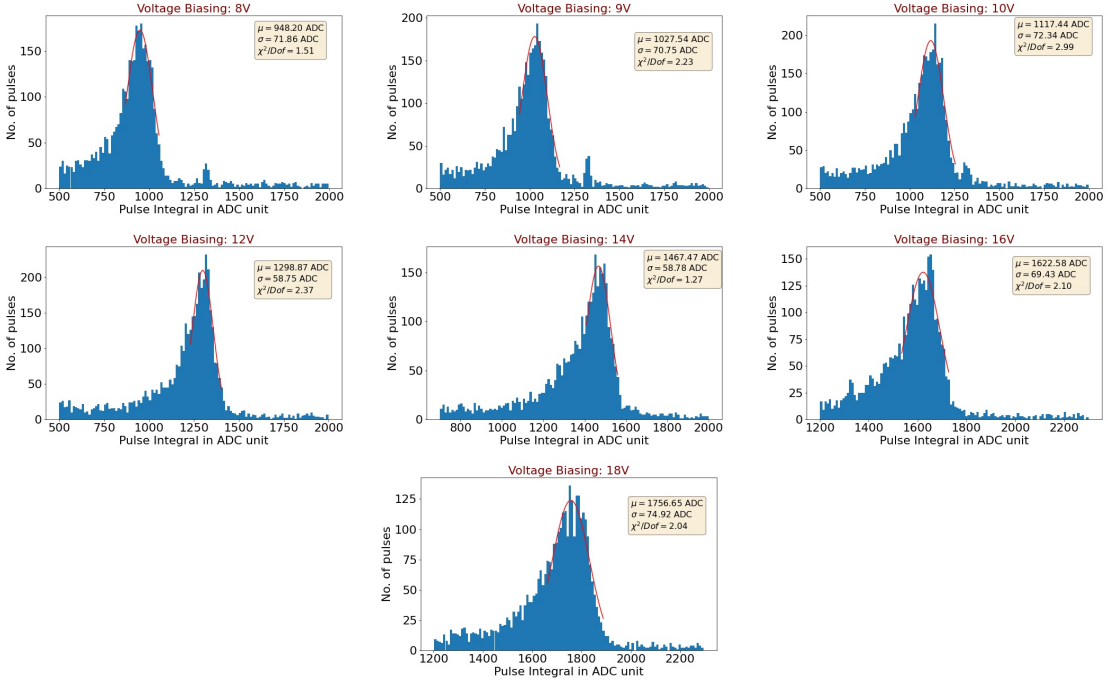

Figure 4.13: Energy spectrum from hybrid detector top channels for different biasing voltages

Figure.4.12 and Fig.4.13 represents ^{241}Am energy spectrum from hybrid detector bottom channels and top channel respectively. This shows increase in energy collection with increase in biasing voltage.

Optimal filter method

Spectrum from bottom channel

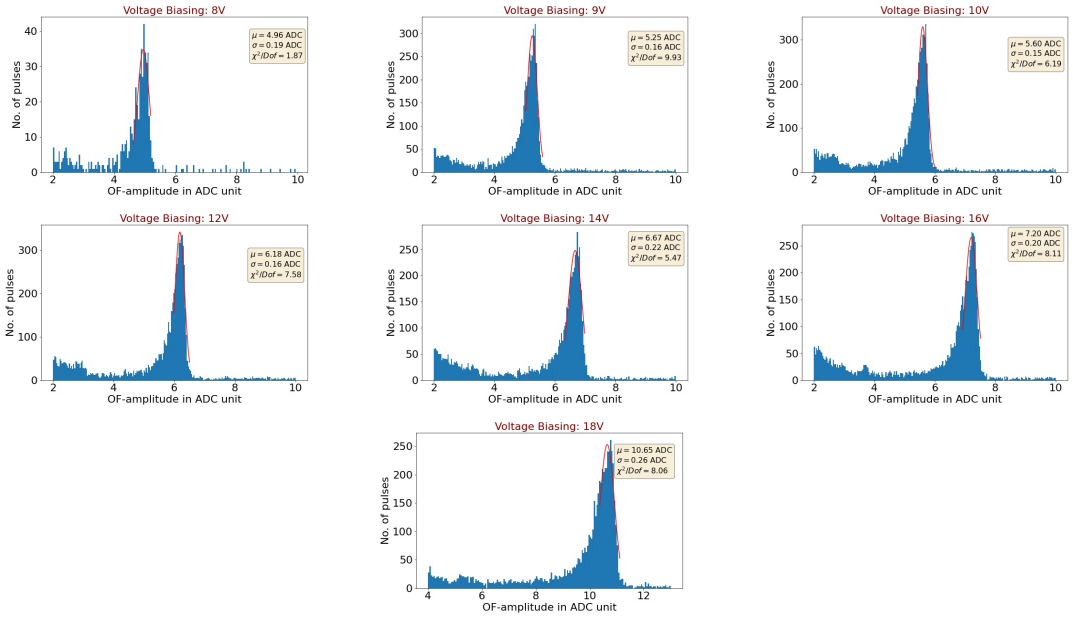

Figure 4.14: Energy spectrum from hybrid detector bottom channels using optimal filter method for different biasing voltage

Spectrum from top channel

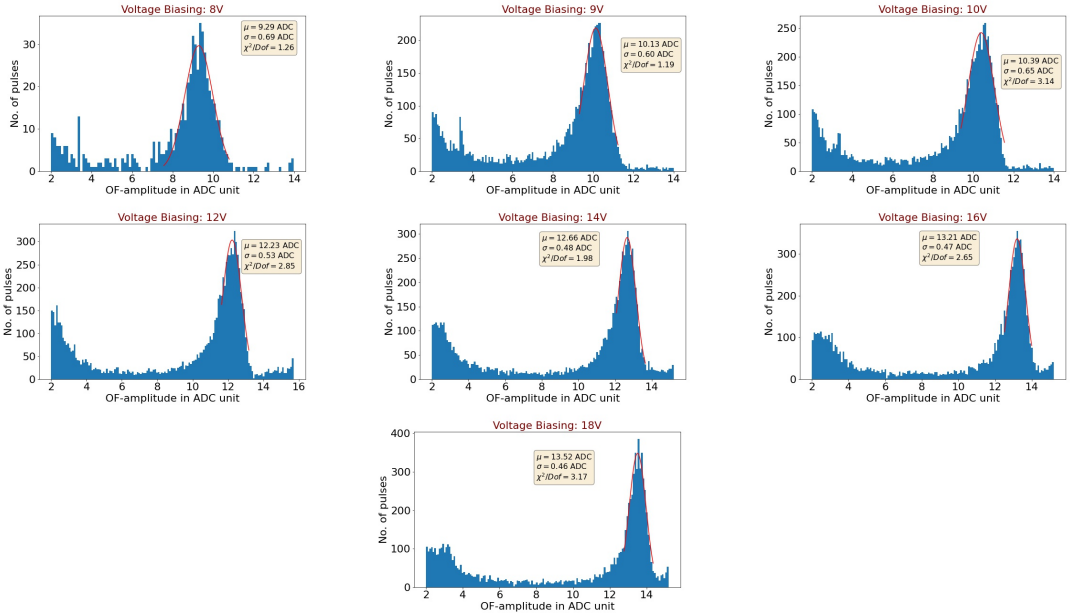

Figure 4.15: Energy spectrum from hybrid detector top channels using optimal filter method for different biasing voltage

Looking through energy spectrum of ^{241}Am it is observed that with increasing biasing voltage, phonon collection is increasing. This is proved in both the sides of the hybrid detector and also this principle is verified using both pulse integral and optimal filter method of energy estimation. Distinct peaks in above figure is fitted and calibrated at 59.54keV of ^{241}Am. From this observation it can be said that both bottom and top channels of the detector are capable of low energy recoil detection.

4.2.2 NTL gain

NTL gain is confirmed in the hybrid detector for both top and bottom channels.

Pulse integral method

Bottom channel

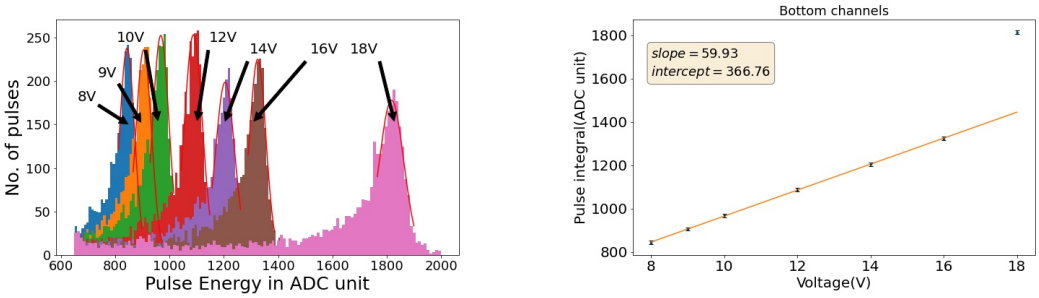

Figure 4.16: Energy spectrum at different voltage (left) and plotting mean energy versus voltage to see linear gain in energy (right) for **bottom channel**

Top channel

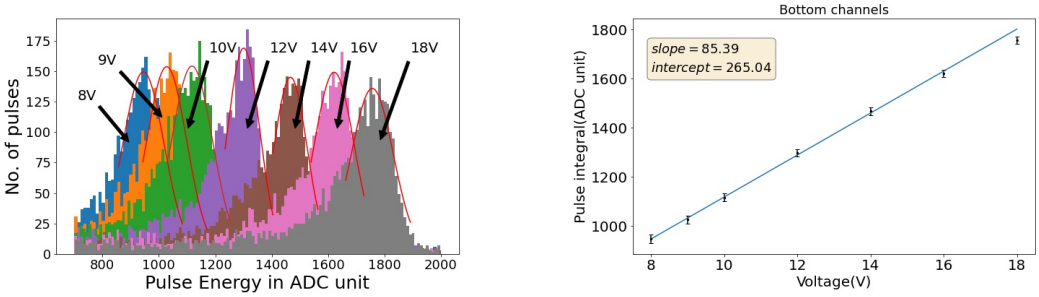

Figure 4.17: Energy spectrum at different voltage (left) and plotting mean energy versus voltage to see linear gain in energy (right) for **top channel**

Above plots clarifies that both top and bottom channel of the hybrid detector shows linear gain in energy with increasing biasing voltage.

Optimal filter method

Bottom channel

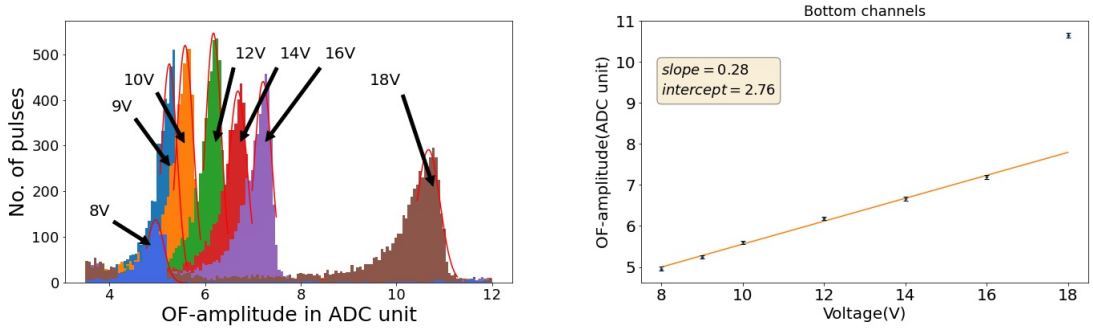

Figure 4.18: Energy spectrum at different voltage (left) and plotting mean energy versus voltage to see linear gain in energy (right) for bottom channel

Top channel

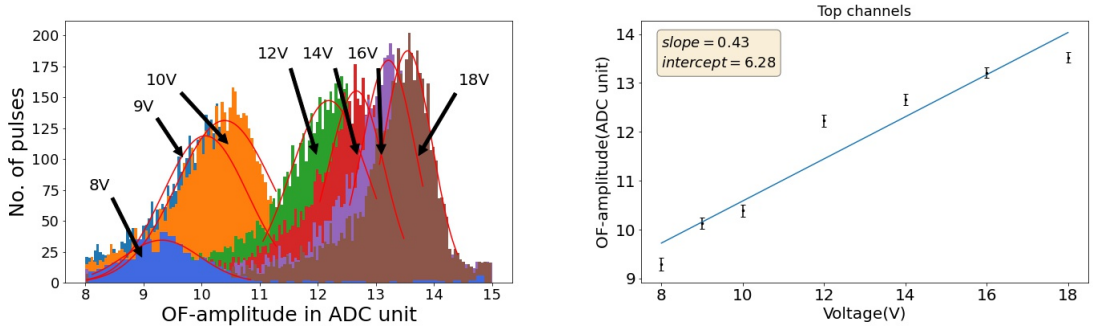

Figure 4.19: Energy spectrum at different voltage (left) and plotting mean energy versus voltage to see linear gain in energy (right) for top channel

Like pulse integral method, linear gain is also observed for both top and bottom channels of the hybrid detector in optimal filter method. Energy plot confirm NTL gain for channels in both the surface of the detector.

4.2.3 Baseline resolution

Baseline resolution is computed like SiHV detector data. Energy spectrum for noise samples are plotted and standard deviation of it taken as baseline resolution.

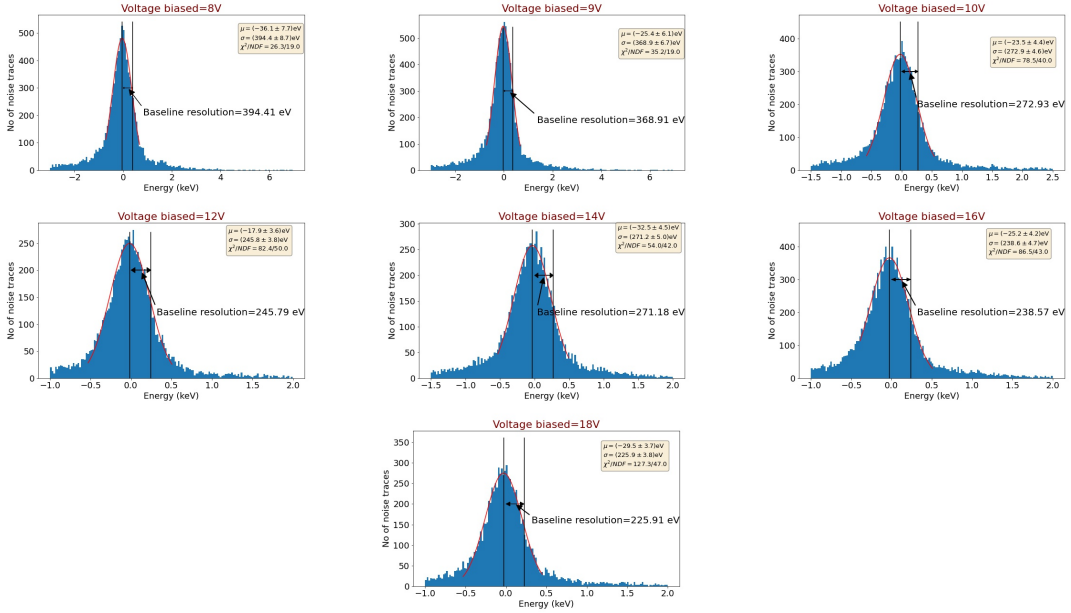

Figure 4.20: Plots for Baseline resolution in **bottom channel**

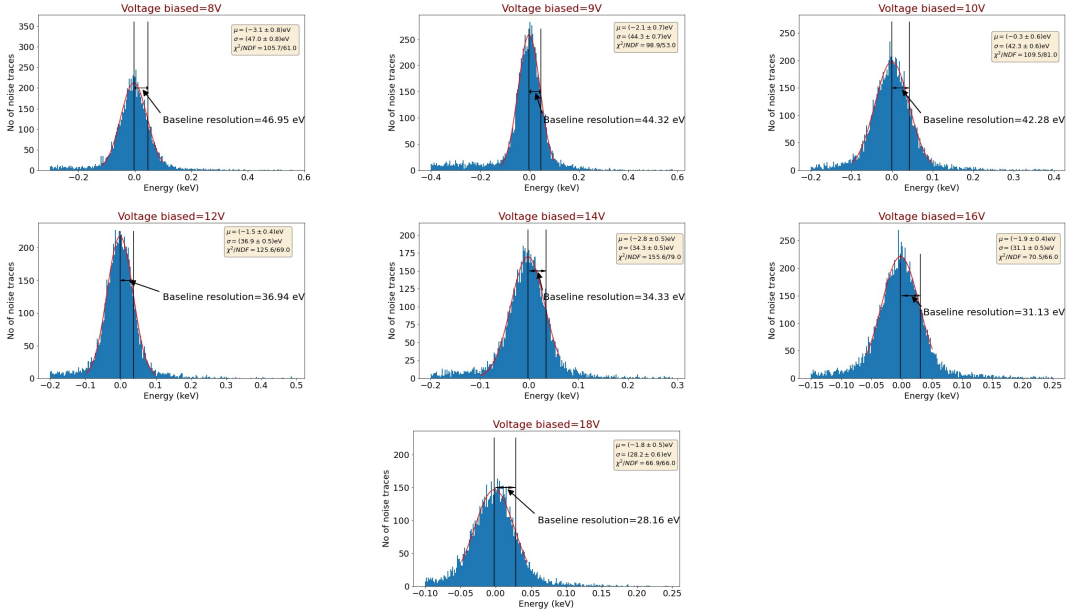

Figure 4.21: Plots for Baseline resolution in **top channel**

Baseline resolution for both top and bottom channel decreases with increase in biasing voltage. Both the plots are fitted with an equation which is made by modifying Eq.4.14. Here detector is biased with maximum of $18V$, we omit leakage current contribution in noise part as leakage current will be minimal at such low voltage.

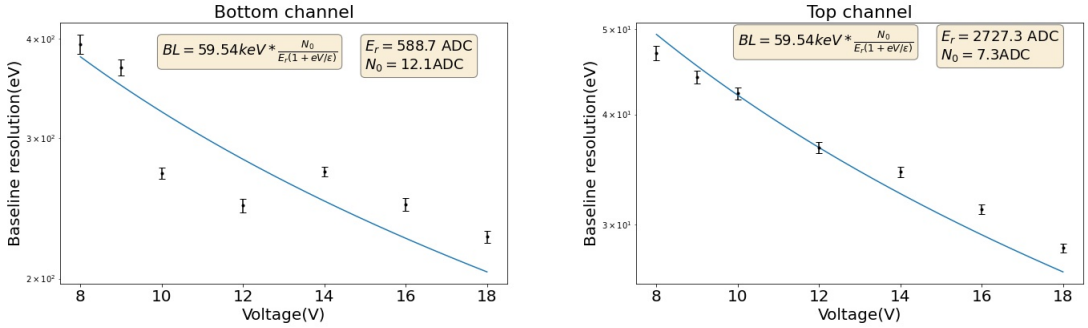

Figure 4.22: Baseline vs voltage for bottom channel (left) and for top channel (right)

Excluding leakage current part from Eq.4.14, baseline resolution equation for hybrid detector will be

$$BR = 59.54 \times \frac{N_0}{E_R + NeV} \tag{4.15}$$

Here 59.54 is multiplied as calibration factor here will be from ^{241}Am peak which is at 59.54 keV. Eq.4.15 is fitted to Fig.4.22 and confirms that our assumption is correct by giving certain value to the defined variables.

4.2.4 Partition plots

Location of source can be found out using partition plots. Partition plots for different biasing voltages are plotted in the Fig.4.23.

We have kept the source over top surface of the detector. With the help of this method we will not be able to locate the Z-coordinate of the source but X-Y coordinates can be measured roughly. As observed from above plots there is an bright spot observed in between channel C to channel D. That suggests the presence of source between those two channels in X-Y coordinate. Same is observed for all biasing voltage says that experiment is performed by keeping the source ^{241}Am in same location for all biasing voltage.

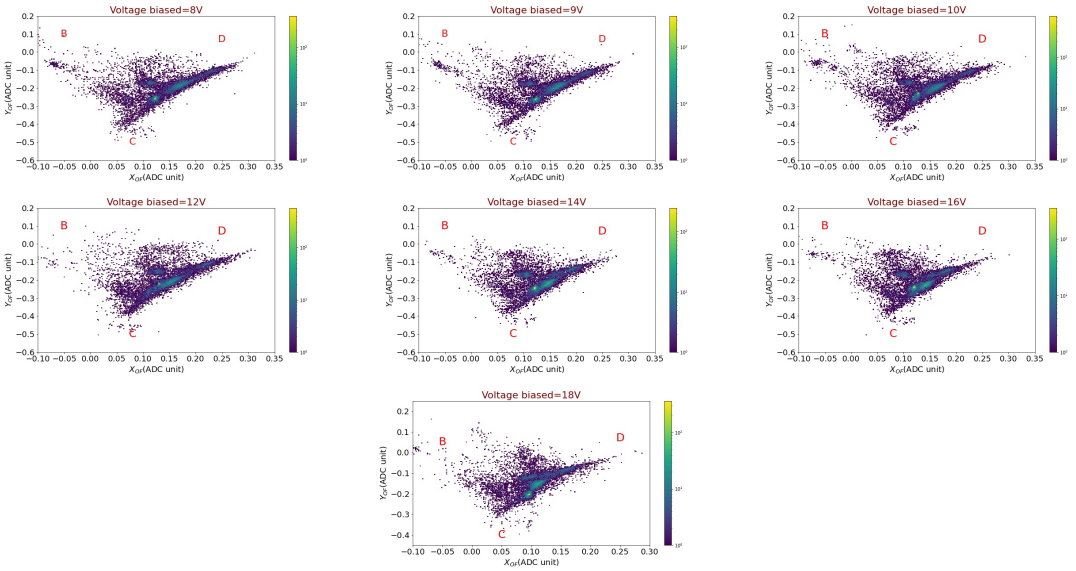

Figure 4.23: Partition plot to identify the location of the source in the hybrid detector based experiment.

4.2.5 ER and NR discrimination

Hybrid detector is made to discriminate between electron recoil and nuclear recoil. As $CE\nu NS$ process is a NR, all the ERs can be treated as background noise and should be eliminated.

As we have studied in Sec.2.1, ionization yield is the distinguishing feature between ER and NR. Which tells that division of energy between charge carrier and prompt phonons are different in ER and NR. Hybrid has the particular feature to measure energy carried by the charge carriers and prompt phonons through top and bottom channel respectively.

Experiment is conducted using hybrid detector with ^{252}Cf, ^{55}Fe and ^{241}Am as source from 24-27 March, 2020 at TAMU. ^{252}Cf, being a γ and neutron emitter produce ER and NR both, placed external to fridge. ^{55}Fe and ^{241}Am, being γ emitter produce ER, placed over top and bottom channels respectively.

Top and bottom channels are calibrated using known source information, and

Voltage(V)	Date	Type	No. of events
0	24 March	Pulse	15675
		Noise	684
		Pulse	18700
		Noise	491
12	24 March	Pulse	21138
		Pulse	20608
		Pulse	17658
		Noise	1369
	25 March	Pulse	17892
		Pulse	20148
		Pulse	24038
		Noise	657
	26 March	Pulse	20651
		Pulse	21608
		Noise	1005
	27 March	Pulse	24750
		Pulse	25155
		Noise	411
18	27 March	Pulse	26353
		Noise	723

Table 4.3: Number of noise and pulse samples in the particular experiment

ionization yield vs energy contained by bottom channels is plotted in keV scale for ER and NR discrimination. Ionization yield is the ratio of energy contained by top channel and bottom channel.

Figure.4.24 shows the presence of two bands. Upper band shows ER events and lower band shows NR events. As you can see band gap is decreasing with increasing bottom channel energy. That means discrimination is effective at lower energy region.

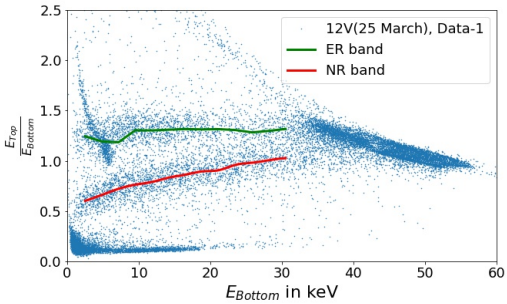

Figure 4.24: ER and NR discrimination plot

4.3 Sapphire detector

Sapphire detector has phonon sensors to detect any interaction, in addition to that sapphire emits light in response to any interaction. So SiHV detector is kept over sapphire to detect the emitted photons and make any prediction for the interacting material (Fig.4.25). ^{241}Am is kept over sapphire detector and ^{55}Fe is kept over SiHV for use as known source.

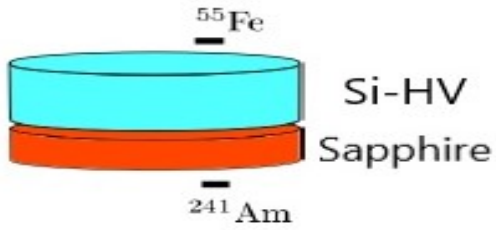

Figure 4.25: Detector setup for sapphire detector

Experiment is done using the configuration similar to Fig.4.25 on 23 December, 2020 at TAMU. Main purpose of this experiment is to observe the signal or photons emitted from the sapphire due to any interaction. So experiment is done by biasing SiHV, kept over sapphire, to detect the signal coming from sapphire whereas sapphire is fixed at 0V. Number of pulse and noise samples collected at different voltage is given in Table.4.4.

Date: December 23, 2020			
Biasing voltage (V)		No. of events	
Si-HV	Sapphire	Pulse	Noise
0	0	4901	1103
50V	0	5052	1023
100V	0	6681	1031
-50V	0	5059	1010
-100V	0	5583	1024

Table 4.4: Number of pulse and noise samples collected at different experiments using sapphire detector.

Here data is taken with both positive and negative bias to the detector. Negative bias causes the holes in the detector to move towards the sensor and form source of prompt phonons and hence energy. Voltage is taken at both the bias to observe or

compare prompt phonons production capability of both the charge carriers, electrons and holes.

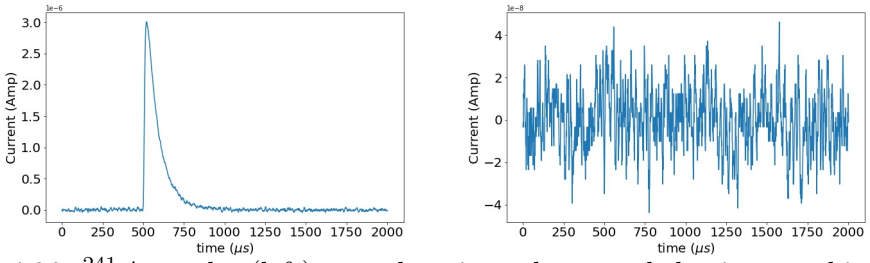

Figure 4.26: ^{241}Am pulse (left), sample noise pulse recorded using sapphire detector

Figure.4.26 represents pulse and noise signal detected using sapphire detector. Measured data is converted into ampere scale by some calibration factor and figure is made. Each trace is measured for 2.004 μs and each data point in trace is noted.

4.3.1 Energy calibration

Energy is calculated using optimal filter method only. Energy plots for different datasets is shown in Fig.4.27. To calibrate the detector we need to identify the source for which the peaks are coming. ^{55}Fe and ^{241}Am are the two sources that is being used in the experiment. To confirm the identity of the source we make use of SiHV detector that is being used in the experiment. So, sapphire and SiHV correlation plots is used to know about the source.

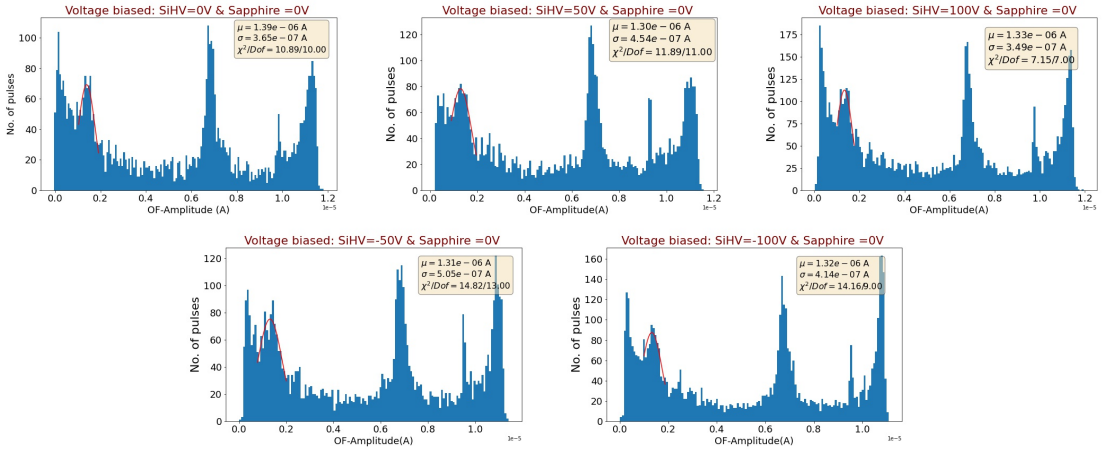

Figure 4.27: Pulse energy histogram using sapphire detector for different biasing voltage.

4.3.2 Sapphire and SiHV energy correlation

If a single event is connected to both the detector by any means, we will see an graphical relation between these two detectors. So we plot SiHV detected energy in X-axis and Sapphire detected energy in Y-axis to find out the relation. ^{241}Am is kept over sapphire detector, it has two distinct peaks 14 keV and 59.54 keV. More the recoil energy in sapphire detector, more energetic photons will be released from sapphire, more will be the phonons detected in sapphire detector sensors, and also higher number photons reach and get detected in SiHV detector and we will get higher signal in SiHV also. This leads to an linear energy relation between sapphire SiHV detector like Fig.4.28. The relation is shown using experimental data also.

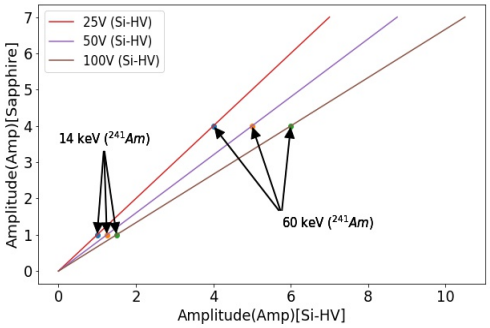

Figure 4.28: Expected correlation plot between sapphire and SiHV detector

In the Fig.4.29 we could not find the linear relation, but we found out ^{55}Fe peak

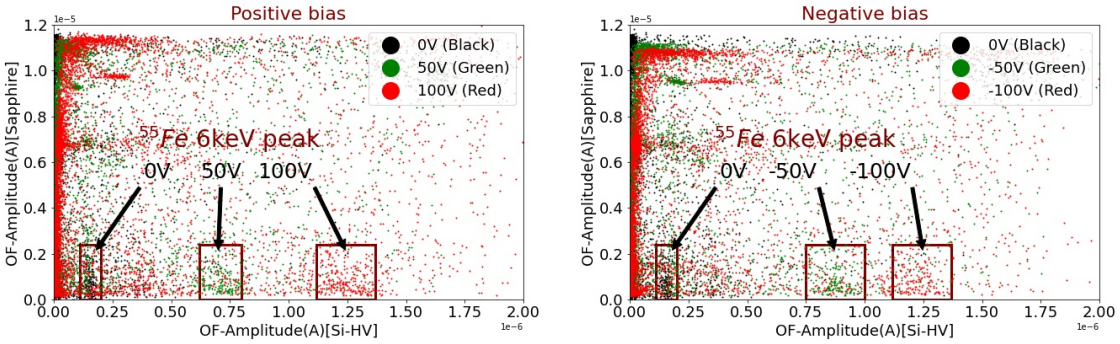

Figure 4.29: experimental observation of sapphire and SiHV correlation plot for positive biasing voltage (left) and negative biasing voltage (right)

seen on SiHV. ^{55}Fe due to very less photon energy can not reach to sapphire detector hence linear relation can not be found out. If we explore the low energy region where ^{241}Am induced photons from sapphire gets detected at SiHV we will possibly find the linear relation.

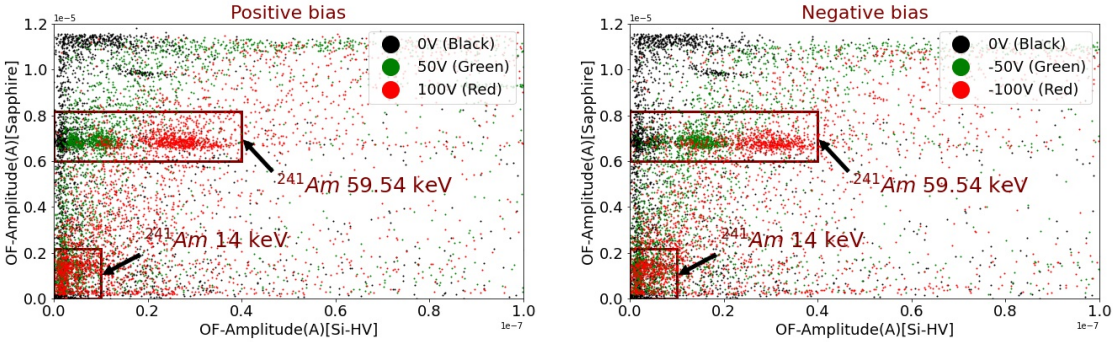

Figure 4.30: experimental observation linear correlation plot as expected from fig.4.28 for positive biasing voltage (left) and negative biasing voltage (right)

Another plot is made by zooming the lower energy regime. As you can see 3 lines were observed at different biasing voltage, black (0V) followed by green (50V) followed by red (100V). Lines also shift rightwards with increasing biasing voltage as NTL gain will increase energy collection hence responsible for shift rightward.

59.54keV signal shows distinct area of detection in SiHV but 14 keV signal shows mixed spectrum. But 59.54keV signal shows saturated pulses in the detector so we

take 14keV signal as our calibration parameter. Baseline resolution is also done using the above calibration.

4.3.3 Baseline resolution

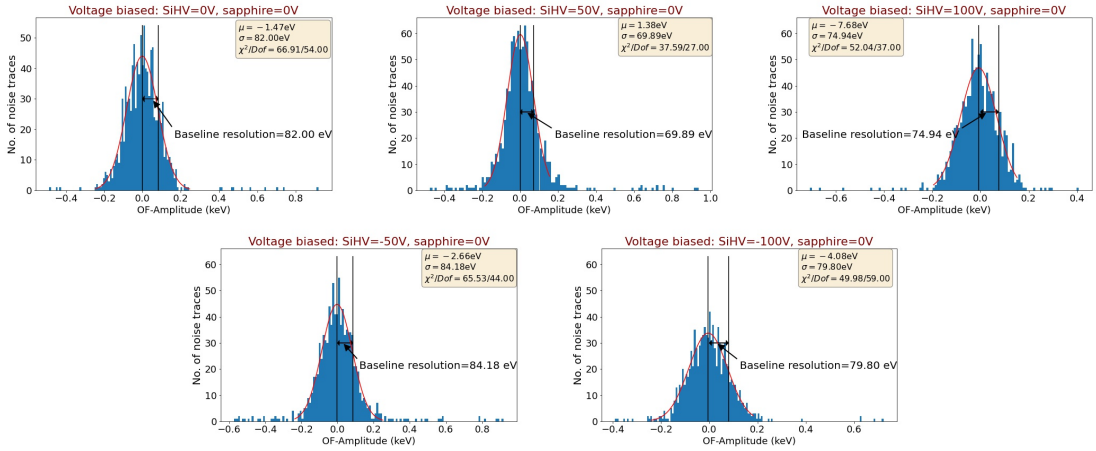

Figure 4.31: Baseline resolution for sapphire detector.

Baseline resolution of sapphire detector at 0V biasing voltage is nearly 80eV. Whereas at 0V biasing baseline resolution for SiHV is coming near 900eV. So resolution is more clearer in sapphire detector. Sapphire detector is more suitable to identify two closed spaced energy peaks.

Chapter 5

Conclusion

Experiment to observe CEνNS will be conducting in next 2 years at MINER. Before that different detectors are being tested to check their properties for low recoil energy detection and background discrimination.

For the testing experiment three types of detectors: SiHV detector, hybrid detector and sapphire detector were studied using known energy source. ^{55}Fe energy source is used for conducting experiment with SiHV detector. From data it is observed that NTL gain is followed by this detector (Fig.4.6 and Fig.4.7). From baseline resolution plot it can be seen that zero noise is not the issue at higher voltages. These observations makes it capable to detect to low energy recoil.

With small modifications in shape of the silicon detector hybrid detector is introduced with an aim to discriminate electron recoil and nuclear recoil. It's capability for low energy recoil detection is observed for both of it's top and bottom channels. In addition, ER and NR discrimination is also observed at 12V biasing voltage (Fig.4.24). Plot also tells that low energy recoils are easy to discriminate comparable to high energy recoils. The detector moves one step forward in reducing noise and hence one step forward in the detection of low energy recoil rare events.

Detectors with different material were also introduced. Sapphire detector is one such. It has an extra feature of emission of light in the material rather than excitation of electrons in semiconductor. Light emission makes energy transfer to phonons more smoother and hence less baseline resolution is expected. Less baseline resolution near to 80 eV (Fig.4.31) is observed for sapphire detector at 0V detector biasing whereas

900 eV (Fig.4.11) is observed for silicon detector . No electron involvement also makes leakage current contribution effectively less to the signal.

With the hope of searching for new physics, science is still developing in making new detectors to get better features for the finding of dark matter like particles. Apart from silicon, germanium detectors are also used in neutrino and dark matter search experiments. Now a days new detectors like Silicon carbide and Gallium arsenide are being made and tested in detector research and development labs. Like $CE\nu NS$ is detected after 40 years of it's prediction we will surely able to detect some rare events with the advanced detector techniques.

Appendix A

Average energy released per fission

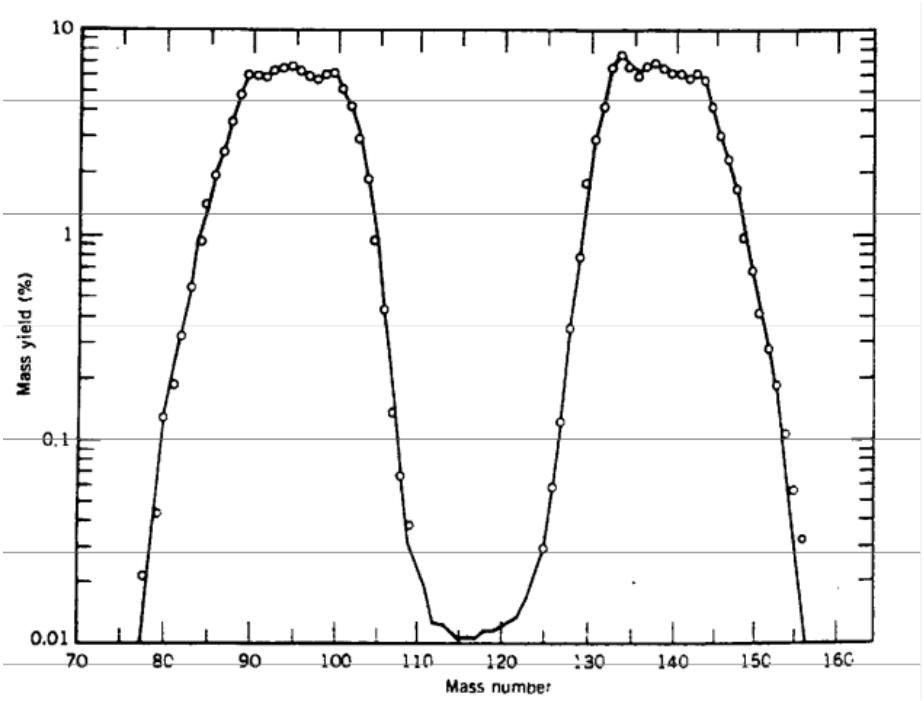

Diagram shows probability of choosing different masses of daughter nucleus in ^{235}U fission reaction. One of the fission reaction for ^{235}U is

$$^{235}U +^{1} n \rightarrow^{236} U^{*} \rightarrow^{141} Ba +^{92} Kr + 3^{1}n$$

Here energy is released from fission of ^{235}U as well as from subsequent decay of daughter nucleus.

1. **B.E/A**:
   - ^{235}U : 7.590MeV
   - ^{141}Ba : 8.326MeV

- ^{92}Kr : 8.512MeV

Energy released in fission is the binding energy difference between reactant and product. That is

$$E_{fission} = \frac{B.E}{A}(^{235}U) * 235 - \frac{B.E}{A}(^{141Ba}) * 141 - \frac{B.E}{A}(^{92}Kr) * 92 \qquad \text{(A.1)}$$

141*8.326+92*8.512-235*7.59=173.288MeV.

2.
- $^{141}_{56}Ba \xrightarrow[3.212MeV]{\beta^-} {}^{141}_{57}La \xrightarrow[2.501MeV]{\beta^-} {}^{141}_{58}Ce \xrightarrow[580.79keV]{\beta^-} {}^{141}_{59}Pr$
- $^{92}_{36}Kr \xrightarrow[5.987MeV]{\beta^-} {}^{92}_{37}Rb \xrightarrow[8.095MeV]{\beta^-} {}^{92}_{38}Sr \xrightarrow[1.945MeV]{\beta^-} {}^{92}_{39}Y \xrightarrow[3.64MeV]{\beta^-} {}^{92}_{40}Zr$

Total energy released from beta decay is $E_\beta = \approx 25.98MeV$

So the total energy computed to be is $E_{total} = E_{fission} + E_\beta = 199.27$MeV.

Average number of ν released per fission

In above reaction number of beta decays is 7. Two more major reaction written to be.

1.
$$^{235}U +^1 n \rightarrow^{236} U^* \rightarrow^{137}_{52} Te +^{97}_{40} Zr + 2^1n$$

- $^{137}_{52}Te \xrightarrow{\beta^-} {}^{137}_{53}I \xrightarrow{\beta^-} {}^{137}_{54}Xe \xrightarrow{\beta^-} {}^{137}_{55}Cs \xrightarrow{\beta^-}{}^{137}_{56} Ba$
- $^{97}_{40}Zr \xrightarrow{\beta^-} {}^{97}_{41}Nb \xrightarrow{\beta^-} {}^{97}_{42}Mo$

Number of beta decay particles is 6.

2.
$$^{235}U +^1 n \rightarrow^{236} U^* \rightarrow^{137}_{55} Cs +^{96}_{37} Rb + 3^1n$$

- ${}^{137}_{55}Cs \xrightarrow{\beta^-} {}^{137}_{56}Ba$
- ${}^{96}_{37}Rb \xrightarrow{\beta^-} {}^{96}_{38}Sr \xrightarrow{\beta^-} {}^{96}_{39}Y \xrightarrow{\beta^-} {}^{96}_{40}Zr \xrightarrow{\beta^-} {}^{96}_{41}Mo$

Number of beta decay particles is 5.

Similarly averaging number of beta decay over all the fission reaction we get 6. So number of neutrino released is also 6.

Appendix B

Power spectral Density

Energy of a signal having voltage "V" is

$$\begin{aligned} E &= \int P(t)dt \\ &= \int_0^T (n(t))^2 dt \\ &= \int_0^T \int\int \tilde{n}(\nu_1)\tilde{n}(\nu_2)e^{-i(\nu_1+\nu_2)t}d\nu_1 d\nu_2 dt \\ &= \int |\tilde{n}(\nu)|^2 d\nu \\ \Rightarrow P &= \frac{E}{T} = \frac{1}{T}\int |\tilde{n}(\nu)|^2 d\nu \\ \Rightarrow J(\nu) &= \frac{dP}{d\nu} = \frac{|\tilde{n}(\nu)|^2}{T} \end{aligned}$$

It is the spectrum of power in frequency space. Power spectral density is a useful tool to find correlation between the events. It has many applications including observing cosmic microwave background. Observing the spectra content of the universe at initial time is predicted.

Bibliography

[1] A. D. Dolgov. "Neutrinos in cosmology". In: *Phys. Rept.* 370 (2002), pp. 333–535. DOI: 10.1016/S0370-1573(02)00139-4. arXiv: hep-ph/0202122.

[2] J. D. Lewin and P. F. Smith. "Review of mathematics, numerical factors, and corrections for dark matter experiments based on elastic nuclear recoil". In: *Astropart. Phys.* 6 (1996), pp. 87–112. DOI: 10.1016/S0927-6505(96)00047-3.

[3] R. Agnese et al. "Projected Sensitivity of the SuperCDMS SNOLAB experiment". In: *Phys. Rev. D* 95.8 (2017), p. 082002. DOI: 10.1103/PhysRevD.95.082002. arXiv: 1610.00006 [physics.ins-det].

[4] David N. Schramm1 Daniel Z. Freedman and David L. Tubbs2. "THE WEAK NEUTRAL :-:5584 CURRENT AND ITS EFFECTS IN STELLAR COLLAPSE". In: ().

[5] Joachim Kopp et al. "Sterile Neutrino Oscillations: The Global Picture". In: *Journal of High Energy Physics* 2013 (Mar. 2013). DOI: 10.1007/JHEP05(2013)050.

[6] Xiaopeng Zhou et.al. "A Search for Solar Axions and Anomalous Neutrino Magnetic Moment with the Complete PandaX-II Data∗". In: *Chinese Physics Letters* 38.1 (Jan. 2021), p. 011301. DOI: 10.1088/0256-307x/38/1/011301. URL: https://doi.org/10.1088/0256-307x/38/1/011301.

[7] Yasaman Farzan and Mariam Tórtola. "Neutrino Oscillations and Non-standard Interactions". In: *Frontiers in Physics* 6 (2018), p. 10. ISSN: 2296-424X. DOI: 10.3389/fphy.2018.00010. URL: https://www.frontiersin.org/article/10.3389/fphy.2018.00010.

[8] Mark David Pepin. "Low-mass dark matter search results and radiogenic backgrounds for the cryogenic dark matter search". PhD thesis. University of Minnesota, 2016.

[9] G. Agnolet et al. "Background Studies for the MINER Coherent Neutrino Scattering Reactor Experiment". In: *Nucl. Instrum. Meth. A* 853 (2017), pp. 53–60. DOI: 10.1016/j.nima.2017.02.024. arXiv: 1609.02066 [physics.ins-det].

[10] *Reactor core setup at MINER*. https://red.library.usd.edu/idea/5/.

[11] Robert Agnese. "Simulating the SuperCDMS dark matter detector and readout". PhD thesis. University of Florida, 2017.

[12] S. Kalbitzer H. Grahmann. "Nuclear and electronic stopping powers of low energy ions with Z 10 in silicon, Nuclear Instruments and Methods". In: 132 (1976), pp. 119–123. ISSN: 0029-554X. URL: https://doi.org/10.1016/0029-554X(76)90720-5..

[13] Adam J. Anderson. "A search for light weakly-interacting massive particles with SuperCDMS and applications to neutrino physics". PhD thesis. Massachusetts institute of technology, 2015.

[14] Allison blair kennedy. "SuperCDMS prototype detector design and testing". PhD thesis. University of Minnesota, 2017.

[15] H. Neog et al. "Phonon-mediated High-voltage Detector with Background Rejection for Low-mass Dark Matter and Reactor Coherent Neutrino Scattering Experiments". In: (2020). arXiv: 2006.13139 [physics.ins-det].

[16] *Numpy Python Description*. https://numpy.org/doc//.

[17] *Scipy Python Description*. https://docs.scipy.org/doc/scipy/reference/.

[18] *Qetpy Python Description*. https://pypi.org/project/QETpy//.

[19] *Matplotlib Python Description*. https://matplotlib.org/stable/contents.html/.

[20] Noah Kurinsky. "The low-mass limit: Dark matter detectors with ev-scale energy resolution". PhD thesis. Stanford university, 2018.